Protein features for assembly of the RNA editing helicase 2 subcomplex (REH2C) in Trypanosome holo-editosomes

Vikas Kumar[1#], Pawan K. Doharey[1#], Shelly Gulati[2#], Joshua Meehan[1], Mary G. Martinez[1], Karrisa Hughes[2], Blaine H.M. Mooers[2*] and Jorge Cruz-Reyes[1*]

[1] Department of Biochemistry and Biophysics, Texas A&M University, College Station, Texas, United States of America.

[2] Department of Biochemistry & Molecular Biology, University of Oklahoma Health Sciences Center, Oklahoma City, Oklahoma, United States of America.

* Corresponding author:

e-mail: cruzrey@tamu.edu

* Correspondence may also be addressed to:

e-mail: blaine-mooers@ouhsc.edu

# These authors contributed equally to this work.

Abstract

Uridylate insertion/deletion RNA editing in *Trypanosoma brucei* is a complex system that is not found in humans, so there is interest in targeting this system for drug development. This system uses hundreds of small non-coding guide RNAs (gRNAs) to modify the mitochondrial mRNA transcriptome. This process occurs in holo-editosomes that assemble several macromolecular *trans* factors around mRNA including the RNA-free RNA editing core complex (RECC) and auxiliary ribonucleoprotein (RNP) complexes. Yet, the regulatory mechanisms of editing remain obscure. The enzymatic accessory RNP complex, termed the REH2C, includes mRNA substrates and products, the multi-domain 240 kDa RNA Editing Helicase 2 (REH2) and an intriguing 8-zinc finger protein termed REH2-Associated Factor 1 (^{H2}F1). Both of these proteins are essential in editing. REH2 is a member of the DExH/RHA subfamily of RNA helicases with a conserved C-terminus that includes a regulatory OB-fold domain. In trypanosomes, ^{H2}F1 recruits REH2 to the editing apparatus, and ^{H2}F1 downregulation causes REH2 fragmentation. Our systematic mutagenesis dissected determinants in REH2 and ^{H2}F1 for the assembly of REH2C, the stability of REH2, and the RNA-mediated association of REH2C with other editing *trans* factors. We identified functional OB-fold amino acids in eukaryotic DExH/RHA helicases that are conserved in REH2 and that impact the assembly and interactions of REH2C. ^{H2}F1 upregulation stabilized REH2 *in vivo*. Mutation of the core cysteines or basic amino acids in individual zinc fingers affected the stabilizing property of ^{H2}F1 but not its interactions with other examined editing components. This result suggests that most, if not all, fingers may contribute to REH2 stabilization. Finally, a recombinant REH2 (240 kDa) established that the full-length protein is a *bona fide* RNA helicase with ATP-dependent unwinding activity. REH2 is the only DExH/RHA-type helicase in kinetoplastid holo-editosomes.

Introduction

Kinetoplastid protozoa including *Trypanosoma brucei* are early-branching eukaryotes that require extensive insertion and deletion of uridylates in most mitochondrial mRNAs (reviewed in 1). This RNA editing is protein-catalyzed and directed by small guide RNAs (gRNAs) with complementarity to fully-edited mRNA. Most editing progresses in blocks that typically overlap and each block is directed by a single gRNA (2). The editing machinery includes multiple subcomplexes: the ~20S catalytic RNA editing core complex (RECC, also called the 20S editosome) and auxiliary editing RNPs. The ~15S REH2-associated complex (REH2C) characterized here includes RNA editing helicase 2 (REH2), REH2-associated protein factor 1 (^{H2}F1), ^{H2}F2, and mRNA substrates and products (3, 4). However, only REH2 and ^{H2}F1 participate in editing. REH2C interacts with a larger accessory editing RNP complex termed the RNA editing substrate binding complex (RESC), which also contains mRNA (5, 6). The presence of mRNA in RESC was confirmed by others (7, 8).

RESC contains two modules that are intimately associated with each other: the gRNA-binding complex (GRBC) typified by the GAP1/GAP2 (alias GRBC2/GRBC1) heterotetramer that binds and stabilizes gRNA, and the more loosely defined RNA editing mediator complex (REMC) (6). REMC is typified by RGG2 and promotes editing progression (8-10). Other mRNA *trans* factors include a subcomplex containing MRB6070 and MRB1590, and RNA helicase REH1 that associate with holo-editosomes via stable or transient RNA contacts, respectively (11-13). The finding that the editing RNPs carry mRNA and gRNA implied that mRNA-gRNA hybrids form on multi-RNP platforms, and that transient addition of the RECC enzyme to the substrate-loaded platforms completes the assembly of the holo-editosome (3-8).

The editing apparatus is further complicated by the occurrence of variants of GRBC, REMC and RECC that may be regulatory (reviewed in 1) but the precise control mechanisms in editing remain unclear. However, the helicase REH2C subcomplex may play an important

71 regulatory role. REH2 is the largest characterized member of the DExH/RNA helicase A (RHA)
72 subfamily of proteins (14). These proteins are monomeric and contain a conserved C-terminal
73 domain cluster with a characteristic auxiliary oligonucleotide-binding (OB fold) domain (3, 14-
74 16). The OB fold in some RNA helicases is known to bind protein regulators or mediate RNA-
75 dependent activation of these enzymes (17). DExH/RHA proteins have a N-terminus with a
76 variable domain organization of less clear function. The N-terminal half of the REH2 carries two
77 predicted double-stranded RNA binding domains: dsRBD1 and dsRBD2 (14). Other
78 characterized DExH/RHA-type proteins that carry two N-terminal dsRBDs are the RNA helicase
79 RHA (aka DHX9) in vertebrates and its orthologous RNA helicase MLE (*maleless*) in flies (18).
80 Recombinant versions of the REH2 N-terminal half and full-size octa-zinc finger ^{H2}F1 formed a
81 stable complex *in vitro* (4). However, ^{H2}F1 is an unusual binding partner of DExH/RHA proteins
82 that typically associate with G-patch proteins (17). A genetic knockdown of ^{H2}F1 prevented
83 RNA-mediated association of REH2 with other editing components and caused fragmentation of
84 REH2 *in vivo*. Those results indicated that ^{H2}F1 is an adaptor protein and may stabilize REH2
85 (4).

86 The current study identified features in REH2 and ^{H2}F1 that affect the binding of these
87 proteins with each other, the stability of REH2, and RNA-mediated stable or transient
88 association of the REH2C subcomplex with other editing components *in vivo*. About 20 different
89 protein variants were examined *in vivo*. Comparisons of the REH2 with other eukaryotic
90 DExH/RHA helicases identified conserved OB fold residues that affect the assembly and
91 interactions of REH2C and are also important in distant processes, namely mRNA splicing in
92 yeast, and the assembly of the dosage compensation complex in fly. ^{H2}F1 upregulation
93 stabilized the large REH2 polypeptide *in vivo*. However, mutation of individual zinc fingers
94 compromised the stabilizing property of ^{H2}F1 but not its association with REH2 or other
95 examined components of the editing apparatus. Most if not all fingers may contribute to REH2

stabilization. Finally, we used a recombinant protein construct to establish that the isolated full-length REH2 (240 kDa) is a *bona fide* RNA helicase enzyme with ATP-dependent unwinding activity. REH2C is most likely an enzymatic editing RNP in kinetoplastid holo-editosomes.

Results

Previous studies revealed that the native REH2C exhibits RNA-mediated interactions with at least two variants of RESC (3-5). These variants contain gRNA and comparable levels of GAP1 and RGG2, that typify GRBC and REMC, respectively. However, these variants differ minimally in their relative content of the canonical MRB3010 in GRBC. Additional variations in protein composition have been reported in purifications of RESC components by different labs (reviewed in 1). Interestingly, native and genetically-induced changes in MRB3010 stoichiometry may be common. While the precise reasons for these changes are unclear, we reasoned that they reflect relevant dynamic changes in the assembly and function of the editing apparatus. In this study, we examined protein features that affect the formation of REH2C, its stable association with RESC components, and its transient contacts with the RECC enzyme. Because the examined helicase-associated RESC variant exhibits substoichiometric MRB3010, we refer to its variant GRBC module as GRBC* (4). Using antibodies made available to us, we have detected other proteins in pulldowns of REH2 that may be part of this RESC variant including both GAP1/GAP2 paralogs and MRB8170. The REH2 pulldowns also contain MRB6070 that was found in a MRB6070/MRB1590 subcomplex that associates via RNA with RESC (11)(S1 Fig.). However, further analysis of relative composition between variants is needed.

Analysis of REH2 mutants *in vivo*

121 We analyzed the importance of specific features of REH2, both in the formation of REH2C
122 and in the association of this subcomplex with other components in holo-editosomes (constructs
123 listed in Fig. 1A). To this end, we expressed a tetracycline (Tet)-inducible REH2 wild-type (WT)
124 construct with a Tandem Affinity Purification (TAP) tag (3) and examined its co-purification with
125 endogenous ^{H2}F1 and GAP1 proteins, of REH2C and GRBC, respectively. We found that ectopic
126 REH2 was able to reconstitute interactions of the native REH2 protein in trypanosomes (Fig. 1B-C,
127 lanes 1-2, respectively). With this system in hand, we tested the assembly of REH2 variants bearing
128 truncations or point mutations in an approach that has been used in other eukaryotic DExH/RHA
129 helicases (16, 19). All REH2 mutants examined were directly compared and normalized to a WT
130 construct used as control. Neither overexpression or depletion of REH2 affects the steady-state
131 level of its binding partner ^{H2}F1 or the examined GRBC proteins (3, 4).
132
133 **Fig. 1. *In vivo* analyses of REH2 variants. (A)** Scheme of REH2 WT (2167 residues) and
134 variants with the examined truncations or point mutations in the N- and C-terminal regions (NTR
135 and CTR). The mutations, affected domains, and predicted molecular weight of the constructs
136 are listed. Identified domains: dsRBD1 and dsRBD2 (double-stranded RNA binding domains 1
137 and 2), CORE (catalytic core RecA1 and RecA2 domains), HA2 (helicase associated helical
138 bundle domain), and OB (OB fold-like domain). **(B-C)** Western blots of IgG pulldowns from
139 extracts to examine the association of tagged REH2 WT or deletion mutants with endogenous
140 ^{H2}F1 and GAP1 (in GRBC*). An uninduced (-Tet) control lane is included. The data are
141 representative of at least three biological replicates for each mutant. A few non-specific species
142 cross-react with the antibodies in some assays. The position of IgG is marked. Sizing markers
143 (M) are in kDa. **(D)** Charts of the relative level of ^{H2}F1 and GAP1 in the pulldowns.
144 Representative assays from panels A-B and other pulldowns in this study were used to plot +/-1
145 SD, *n*=3 for each mutant. The ^{H2}F1/REH2 and GAP1/REH2 ratios in each REH2 mutant were
146 normalized to the ratios in REH2 WT (= 1, in the plot). Assays with signals that were too low

147 were not determined (n.d.). REH2 was often fragmented, so only the full-length polypeptide was
148 scored. Some short deletion mutants were present at higher level than tagged REH2 WT in the
149 induced extracts.
150
151 *N- and C-truncations*. We examined N- and C-terminal regions (NTR and CTR) flanking the
152 catalytic and helicase associated domains RecA1/RecA2 and HA2, respectively, in REH2. We
153 removed sequences in the unique NTR (>1000 residues) in the REH2 variants ∆N and ∆Nds. Next,
154 we removed the CTR after the OB fold (123 residues) or from the OB fold (260 residues) in the ∆AOB
155 and ∆OB variants, respectively. REH2 and its orthologs in kinetoplastids carry the longest N terminus
156 in the known DExH/RHA-type helicases (~1300 residues in REH2 from *T. brucei*) (14). Direct
157 comparisons with the REH2 WT construct showed that the examined N- and C-resections reduced
158 the association of the shortened REH2 polypeptides with ^{H2}F1 and GAP1 proteins (Figs. 1B-D). This
159 suggested that both termini of REH2 may contribute to the normal assembly of REH2C and its RNA-
160 mediated interactions with other editing components *in vivo*. The dsRBDs, the OB fold, and
161 undefined features in the N and C termini may be involved. It is also conceivable that the examined
162 sequence resections may impact the global conformation of REH2, thereby indirectly affecting its
163 protein interactions. In that case, the normal REH2 interactions in the editing apparatus may be
164 sensitive to overall changes in the integrity or conformation of REH2. A comparison of REH2 ∆N and
165 ∆Nds in whole-cell and enriched-mitochondrial extracts indicated that these large truncations do not
166 prevent mitochondrial import (S2 Fig). Because the CTR includes a potentially regulatory OB fold in
167 DExH/RHA-type RNA helicases (16), we focused on this domain in the subsequent studies of REH2.
168
169 *Point mutations*. Our structural searches of the OB fold-like domain in REH2 using Phyre2
170 (20) found the best agreements of the REH2 OB fold with structures of yeast ADP-bound Prp43p
171 helicase and *Drosophila* RNA helicase MLE in a complex with RNA and ADP-Alf4 (4, 16, 18, 21).

172 Prp43p is a bi-functional helicase in mRNA splicing and ribosome biogenesis (15, 22). The helicase
173 MLE remodels roX RNA substrates to promote assembly of the dosage compensation complex in
174 *Drosophila* (18). We examined specific residues in the predicted OB fold of REH2 that seem to be
175 conserved in the DExH/RHA helicases mentioned above (Fig. 2 A-D). OB point mutations were
176 compared to two controls: REH2 WT and a mutation in dsRBD2 (dsR) that reduces the association of
177 REH2 with GAP1, gRNA and mRNA (Fig. 2A, lanes 1 and 2, respectively) (3). The β1−β2 and β4−β5
178 loops in the OB fold may include determinants in nucleic acid recognition (Fig. 2D) (16, 18). In
179 helicase Prp43p, mutation of K704 (β4−β5 loop), which is exposed to the solvent in the Prp43p
180 structure, decreased the RNA affinity and ATPase activity of the helicase *in vitro* (16). Sequence
181 alignments and a homology model derived from the structure of Prp43p matched K704 in Prp43p
182 with R2023 in the predicted β4−β5 loop in REH2 (S3 Fig)(4). We also examined R1979 in REH2 that
183 is not conserved in Prp43p and may serve as an internal control. Pulldowns of the R1979A and
184 R2023A mutants suggest that neither mutation alters the association of REH2 with ^{H2}F1 (Figs. 2A-C).
185 R1979A did not appear to affect the REH2 association with GAP1. However, R2023A caused a
186 moderate decrease in the association with GAP1, implying that at least R2023A could be disruptive
187 in trypanosomes.

188 In helicase MLE, several residues in the OB fold bind to specific uridylates in U-rich
189 sequences in roX transcripts. Mutation of some of these residues impaired RNA binding by MLE *in*
190 *vitro* or the proper localization of MLE in chromosomes (18). Sequence alignments and homology
191 models indicated that the residues H1032 and K1033 in MLE likely represent residues H1998 and
192 R1999 in the predicted β3−β4 loop in the OB fold in REH2 (Fig. 2D; S4 Fig)(21). The H1998E mutant
193 appeared to retain a normal association with ^{H2}F1 but exhibited a moderate decrease in association
194 with GAP1. In contrast, R1999E either alone or together with H1998E (98/99) exhibited a more
195 robust decrease (over 60%) in association with both ^{H2}F1 and GAP1 (Fig. 2A-C). This indicated that
196 H1998 and R1999 contribute to the assembly of the REH2 helicase with other editing components.

197 However, R1999 has a higher impact on such interactions than the adjoining H1998. As expected,
198 the dsR mutant used as a control exhibited a strong decrease in association with GAP1. However,
199 the dsR mutation did not seem to affect the association of REH2 with ^{H2}F1 (Figs. 2A, 2C). Pulldowns
200 of the mutants were normalized to the REH2 WT control as in Fig. 1.
201
202 **Fig. 2. *In vivo* analyses of REH2 variants.** Western blots of IgG pulldowns as in Fig. 1 to
203 examine the association of endogenous ^{H2}F1 and GAP1 (in GRBC*) with tagged REH2 WT or
204 variants with point mutations at: **(A)** the OB fold domain at R1979A (1979), H1998E (1998) and
205 R1999E (1999). The previously characterized dsR mutant with an inactivating double mutation
206 in the dsRBD2 was included for comparison (3). A few non-specific species crossreact with the
207 antibodies in some assays; and **(B)** the OB fold domain at double 1998/1999 (98/99) or single
208 mutation at 2023. **(C)** Charts of the relative levels of ^{H2}F1 and GAP1 in the pulldowns. Assays
209 from panels A-B and biological replicate pulldowns in this study were used to plot +/-1 SD, *n*=2
210 or *n*=3 for each mutant. The ^{H2}F1/REH2 and GAP1/REH2 ratios in each REH2 mutant were
211 normalized to the ratios in REH2 WT (= 1, in the plot). **(D)** Secondary structure prediction of the
212 OB fold with α-helix (cylinders) and β-strand (arrows) elements, and the position of point
213 mutations examined indicated by arrows.
214
215 Table 1 summarizes observed effects of the examined mutations in REH2 on its association
216 with ^{H2}F1 and GAP1. While large protein truncations in REH2 may alter the global conformation of
217 the polypeptide, relevant point mutations in REH2 are more likely to cause specific functional effects.
218 Our systematic mutagenesis of REH2 suggests an intricate interaction network including features
219 across both N- and C- terminal regions of REH2 that affect the assembly of REH2C, and the
220 association of this subcomplex with GAP1-associated RNPs *in vivo*. Remarkably, these observations
221 also indicate that equivalent residues in the auxiliary conserved OB fold domain in DExH/RHA

222 helicases function in disparate RNA processes in the taxonomically distant species of trypanosomes,
223 yeast, and fly.

224 **Table 1. Association of REH2 constructs with ^{H2}F1 and GAP1**

REH2-TAP variant	Association in pulldown		Reference
	^{H2}F1	GAP1	Construct described
WT	control*	control*	23
ΔN	decreased	decreased	This study
ΔNds	decreased	decreased	This study
ΔOB	decreased	decreased	This study
ΔAOB	decreased	decreased	This study
dsR	control-like †	decreased	3
1979	control-like	control-like	This study
1998	control-like	decreased	This study
1999	decreased	decreased	This study
98/99	decreased	decreased	This study
2023	control-like	decreased	This study

* The WT construct served as positive control to assess relative association of mutant constructs.
225 † Comparable to the level observed with the WT construct.
226

227 ## Analysis of ^{H2}F1 mutants *in vivo*
228
229 To analyze specific features of the ^{H2}F1 zinc finger protein in trypanosomes, we expressed a
230 Tet-inducible tagged ^{H2}F1 WT construct and examined its association with endogenous REH2, GAP1
231 and REL1 proteins. REL1 is a subunit of the editing enzyme RECC. We found that the tagged ^{H2}F1
232 WT was able to reconstitute interactions of the native ^{H2}F1 protein in trypanosomes (Fig. 3). Notably,
233 expression of the ectopic ^{H2}F1 WT increased the steady-state level of endogenous REH2 compared
234 to a control lane without tetracycline (Fig. 3A, lanes 1-2; Fig. 3B). As a control to mark the position of
235 REH2 we used a reported RNAi-based knockdown of ^{H2}F1 that decreases the level of endogenous
236 REH2 (Fig. 3A, lanes 5-7; Fig. 3B)(4). The contrasting effects of the upregulation and downregulation
237 of ^{H2}F1 on the endogenous REH2 are consistent with the idea that ^{H2}F1 stabilizes REH2 *in vivo*. We
238 examined the distribution of REH2 and ^{H2}F1, and canonical proteins in RESC and RECC, in
239 sedimentation analyses of mitochondrial extract (S5 Fig). REH2 is heterodispersed as shown before
240 (23) and overlaps with ^{H2}F1 in the gradient. However, the relative abundance of these proteins at

241 high and low densities differs substantially. It is possible that the association between REH2 and ^{H2}F1
242 or their stoichiometry in REH2C varies *in vivo*. Additional studies will be necessary to examine these
243 possibilities.
244
245 **Fig 3. Effect of expressing ^{H2}F1 WT or Zn5 C2>A2 on the REH2 steady-state abundance.**
246 Figure annotations use short acronyms for each mutant in the form: Z*X*. **(A)** Western blots of
247 extracts with tagged ^{H2}F1 WT (lanes 1-2) or Z5 C2>A2 (Z5; lanes 3-4). Control assays include
248 lanes without Tet-induction. Control lanes with a reported ^{H2}F1-RNAi construct mark the position
249 of the endogenous REH2 and ^{H2}F1. The RNAi lanes show the induced decrease of ^{H2}F1 and
250 concurrent fragmentation of REH2 full-length. Hash marks indicate full-length and two prominent
251 fragments of REH2 (4). GAP1 was used as a loading control in all assays in this panel.
252 Molecular size markers (M). A typical C2H2 zinc finger domain fold is depicted with core
253 cysteine substitutions C2>A2 (arrows), other conserved residues, and variable residues (black
254 circles). **(B)** Charts of the relative levels of endogenous REH2 full-length in the extracts +/-1 SD,
255 *n*=3. Induced/uninduced ratios of REH2 for each construct were further normalized to GAP1. **(C-**
256 **D)** IgG pulldowns of WT and Z5 constructs showing association with endogenous REH2, GAP1,
257 REL1, and endogenous ^{H2}F1. REL1 is examined by radiolabeled self-adenylation. Other
258 proteins are examined as in panel A. Non-specific species (*) may represent fragments of the
259 tagged protein that react with the antibodies. **(E)** Charts of the relative levels of REH2, GAP1
260 and REL1 in the pulldowns +/-1 SD, *n*=3. The ratios (protein/tagged-bait) in the Z5 mutant were
261 normalized to ratios in the ^{H2}F1 WT construct.

262
263 To determine if the stabilizing effect of ^{H2}F1 requires one or more zinc finger (Znf) domains,
264 we introduced amino acid substitutions that either disrupt the canonical fold of the domain (by
265 replacing the canonical residues) or eliminate the positive charge (by replacing various basic
266 residues with neutral residues) in individual fingers of the ectopic construct. The examined ^{H2}F1

267 mutants are summarized in Table 2. The location of the fingers and the examined substitutions
268 (between 2 and 6 basic residues per finger) in the full sequence of ^{H2}F1 are shown in S6 Fig. All
269 ^{H2}F1 mutants examined were directly compared and normalized to a WT construct used as
270 control in all panels. This enabled the separation of mutants in multiple panels.

271 **Table 2. ^{H2}F1 mutants with reduced ability to stabilize REH2 *in vivo***

^{H2}F1-TAP variant	Endogenous REH2 *Steady-state level*	Figures using this construct
WT	**Increased***	Figs. 3, 4 and 5
Znf5 C2>A2	no change †	Fig. 3
Znf1 R/K>A	no change	Fig. 4
Znf2 R/K>A	no change	Fig. 4
Znf3 R/K>A	no change	Fig. 4
Znf4 R/K>A	no change	Fig. 5
Znf5 R/K>A	no change	Fig. 4
ΔN	no change	Fig. 5
ΔC	no change	Fig. 5

* ^{H2}F1-WT ectopic expression increased the level of endogenous REH2
272 † No change (i.e., level within stardard deviation for at least two biological replicates)
273
274 *Canonical cysteine residues*. We changed two cysteines to two alanines (C2>A2) to disrupt
275 the native conformation of the predicted zinc fingers (Fig. 3A). We began by disrupting Znf5 because
276 of its significant homology to a reported dsRNA-bound C2H2 zinc finger domain structure (4, 14, 24).
277 Mutants are referred to in the text by the acronym in the general form Znf*X*. A shorter version of the
278 acronym is used in the figure annotations. The resulting mutant protein Znf5 C2>A2 did not induce an
279 evident increase in the steady-state level of endogenous REH2 as we found after expressing the
280 ^{H2}F1 WT construct. This was evident in direct comparisons of extracts that contain similar levels of
281 ectopic ^{H2}F1 protein, WT or Znf5 C2>A2 (Fig. 3A, lanes 1-4; Fig. 3B). To examine whether the lack of
282 Znf5 affected the association of ^{H2}F1 with other editing components, we performed IgG pulldown
283 assays of tagged ^{H2}F1. These assays showed that the ^{H2}F1 WT and Znf5 C2>A2 variants similarly
284 associated with endogenous helicase REH2, GAP1 and REL1 ligase (Figs. 3C, 3E). Notably,
285 pulldowns of both tagged ^{H2}F1 WT and Znf5 C2>A2, contain endogenous ^{H2}F1 (Fig. 3D). The above

286 data suggest that Znf5 is not essential for the normal association of ^{H2}F1 with other editing
287 components.
288 We also attempted to generate a ^{H2}F1 variant bearing a triple C2>A2 substitution in Znf6,
289 Znf7 and Znf8. However, expression of this construct was unstable and eventually lost in culture.
290 Together, the observations above suggest that ^{H2}F1 may require a full complement of zinc fingers in
291 their native conformation to stabilize REH2 but not to associate with the examined editing
292 components.
293
294 *Variable basic residues*. Because the native conformation of the zinc fingers seems to be
295 required for ^{H2}F1 to stabilize REH2 we introduced mutations that decrease the positive charge in the
296 zinc fingers yet likely to retain native conformation (25). We expressed ^{H2}F1 variants to test the role
297 of several basic residues around the core residues that are mostly located between the second
298 cysteine and the first histidine (Fig. 4A) (26). Specifically, we introduced R/K>A substitutions
299 (between 2 and 6 per finger) to decrease the positive charge in the zinc fingers and to remove
300 potential charge-charge interactions with REH2 or associated RNAs. As above, we use in the text the
301 acronym in the general form Znf*X* but a shorter version of the acronym in the figures. Our functional
302 analyses of Znf1, Znf2, Znf3 or Zn5 R/K>A variants showed that the loss of positive charge in any of
303 these zinc fingers reduced the ability of ^{H2}F1 to induce the accumulation of intact endogenous REH2
304 in extracts (Figs. 4B-C). However, these mutations did not prevent the association of ^{H2}F1 with
305 REH2, GAP1 and REL1 (Figs. 4D-F). These expressed ^{H2}F1 variants also co-purified with
306 endogenous ^{H2}F1 at a level comparable to the WT construct (Figs. 4D, 4F). The data above indicated
307 that the wildtype and R/K>A variant proteins associated similarly with the examined editing
308 components. Overall, ^{H2}F1 may require that most zinc fingers retain their native conformation and
309 positive charge to efficiently increase the stability of REH2. However, the loss of the native
310 conformation or positive charge in individual fingers does not preclude the assembly of ^{H2}F1 in the
311 REH2C, or the association of this subcomplex with the examined editing components. Detection of

312 endogenous ^{H2}F1 in our pulldowns suggest the presence of ^{H2}F1 multimers. Pulldowns treated with
313 an RNaseA/T1 mixture suggest that the association between tagged ^{H2}F1 and endogenous ^{H2}F1 is
314 RNase-resistant (S7 Fig.). However, further studies using isolated recombinant proteins are needed
315 to establish direct protein contacts between ^{H2}F1 monomers as was shown between REH2 and ^{H2}F1
316 (4).
317
318 **Fig. 4. *In vivo* analyses of ^{H2}F1 variants with reduced positive charge in Znf1, Znf2, Znf3**
319 **or Znf5 (variable residues R/K>A).** Figure annotations use a shorter acronym of the mutant in
320 the form: Z*X*. **(A)** Cartoon of ^{H2}F1 (524 residues). Multi-sequence alignment of the eight C2H2
321 zinc fingers, indicating the core cysteines and histidines (boxes) and R/K>A substitutions of
322 variable residues (between 2 and 6) in each finger (open circles). The C2H2 zinc finger domain
323 fold is depicted as in Fig. 3. In this case, the arrows illustrate three variable residue substitutions
324 R/K>A. **(B)** Western blots of extracts as in Fig. 3A of induced tagged ^{H2}F1 WT and Z1, Z2, Z3
325 and Z5 R/K>A mutants or uninduced control. GAP1 was used as a loading control (lanes 1-7).
326 **(C)** Chart of steady-state level of endogenous REH2 full-length in extracts with each construct
327 as in Fig. 3B. **(D-E)** Western blots and self-adenylation reactions of IgG pulldowns of ^{H2}F1 WT
328 and Z1, Z2, Z3 and Z5 R/K>A mutants showing association with endogenous REH2, ^{H2}F1,
329 REL1 and GAP1. Non-specific species in pulldowns (*) are indicated. (**F)** Charts of the relative
330 levels of associated endogenous proteins in the pulldowns +/-1 SD, *n=2* or *n*=3, as in Fig. 3.
331 The ratios (protein/tagged-bait) in the mutants were normalized to ratios in the ^{H2}F1 WT
332 construct.
333
334 *N- and C-truncations*. Because mutagenesis of the tested Znf domains did not prevent the
335 association of ^{H2}F1 with other editing components *in vivo*, we asked if fragments of ^{H2}F1 retain these
336 interactions. To test this question, we expressed N- or C-terminal fragments including Znf1-to-Znf3
337 (termed ΔC) or Znf4-to-Znf8 (termed ΔN) that span 49% and 51% of the ^{H2}F1 polypeptide chain,

338 respectively (Fig. 5A, bottom). These two fragments exhibited minimal or no association with the
339 examined endogenous REH2, ^{H2}F1, or REL1 ligase (Figs. 5A). These mutants were directly
340 compared with the ^{H2}F1 WT and Znf4 R/K>A constructs. We note that while Znf4 R/K>A was
341 examined separately from the R/K>A variants in Fig. 4, all R/K>A mutants are normalized to the ^{H2}F1
342 WT construct that was included in all gels. The Znf4 R/K>A and other Znf R/K>A mutations in the
343 current study retained all tested interactions that are observed with the ^{H2}F1 WT control. However,
344 the ΔN and ΔC constructs failed to establish basic interactions with the tested editing components.
345 Because the native REH2C subcomplex carries mRNA (4), we wondered if the ^{H2}F1 ΔN and ΔC
346 constructs also fail to co-purify with mRNA. To this end, we quantitated the relative content of
347 mitochondrial transcripts in the pulldowns of the WT, ΔN, and ΔC constructs in biological replicate
348 experiments that were performed in triplicate (Fig. 5B). The examined mitochondrial transcripts
349 include examples of unedited, edited, and never-edited mRNA, the never-edited mRNA ND4, and
350 ribosomal RNA 9S. We also examined cytosolic transcripts (Tubulin, 1400 and 1390) to score non-
351 specific RNA interactions of editing subcomplexes as in previous pulldown studies (5). Relative to the
352 ^{H2}F1 WT control used for normalization, both ΔN and ΔC pulldowns exhibited a dramatic loss in
353 bound mitochondrial mRNAs (Fig. 5B, upper and middle panels). Interestingly, the level of cytosolic
354 mRNAs was similar in the ΔN and WT proteins but dramatically less in the ΔC variant. The later
355 variant lost most examined RNA interactions: specific and non-specific. An exception may be
356 mitochondrial RNA 9S. We also compared the relative impact of the ΔN and ΔC deletions with a
357 more discrete alteration in Znf4 R/K>A (Fig. 5B, lower panel). The level of mitochondrial RNAs in the
358 Znf4 pulldown was similar to that of the ^{H2}F1 WT control. However, the level of cytosolic transcripts
359 decreased ~70 fold in Znf4 R/K>Ala. The independent pulldowns and RNA quantitation in three
360 equivalent experiments showed consistent results in the protein interactions and RNA content of
361 these ^{H2}F1 constructs. The above data indicated that the tested ^{H2}F1 fragments appear to have lost
362 the normal direct interaction of ^{H2}F1 WT with REH2 in REH2C, and the normal RNA-dependent

363 association of ^{H2}F1 WT with other examined proteins in the editing apparatus. Quantitation of the
364 examined transcripts in the input extracts (including those used in the pulldowns in Figs. 5A-B)
365 confirmed that the observed dramatic loss in RNA association with ΔN and ΔC constructs was not
366 due to large changes in the transcript level at steady state (S8 Fig.). The above observations indicate
367 that features in both termini of ^{H2}F1 are required for efficient association of mitochondrial transcripts
368 in the pulldowns of ^{H2}F1. The ^{H2}F1 ΔN construct used a heterologous mitochondrial leader sequence
369 (see methods and S1Table). A comparison of ^{H2}F1 ΔN and ΔC in whole-cell and enriched-
370 mitochondrial extracts suggest that ^{H2}F1 ΔN localizes to mitochondria efficiently. However, the import
371 or retention of ^{H2}F1 ΔC into mitochondria may be relatively compromised. At least some import of the
372 ^{H2}F1 ΔC construct may occur in comparison with a control cytosolic marker in whole-cell and
373 enriched-mitochondrial extracts (S2 Fig.). This indicates that this C-terminal truncation affected both
374 the ^{H2}F1 association with all examined transcripts (including cytosolic) and somehow also its
375 mitochondrial import. Finally, the more discrete alteration in Znf4 R/K>A may have caused a relatively
376 mild decrease in RNA affinity that mostly affected weak, non-specific interactions, e.g., by cytosolic
377 RNA in the pulldowns of ^{H2}F1.
378
379 **Figure 5. *In vivo* analyses of ^{H2}F1 terminal deletion and Znf4 mutants. (A)** IgG pulldowns of
380 N and C truncation mutants (ΔN and ΔC) that removed fingers 1-to-3 and fingers 4-to-8,
381 respectively, and the Z4 R/K>A variant. Association of the constructs with endogenous REH2,
382 ^{H2}F1 and REL1 was examined. Biological replicates of these assays suggest a similar quality
383 and loading of samples in the pulldowns. Cartoon of ^{H2}F1 with zinc fingers and a line marking
384 the N and C truncations. **(B)** qRT-PCR quantitation of transcripts in the pulldowns in panel A.
385 dCq of IgG pulldowns of tagged protein (induced extract) normalized to a mock pulldown
386 (uninduced extract) [dCq = $2^{(\text{test Cq} - \text{mock Cq})}$] for each construct. The mutant proteins were then
387 normalized to the tagged WT protein. All values took into account the recovery of tagged protein

388 in each pulldown in panel A. Three independent biological replicates with Cq average values
389 and one standard deviation (+/-1 SD, *n*=3) were plotted. Non-specifically associated cytosolic
390 transcripts differed substantially in pulldowns of different mutants, so these transcripts were not
391 used as reference. Mitochondrial unedited (UE) and edited (ED) and cytosolic RNA transcripts
392 are indicated. RPS, Murf, and 9S are abbreviations for RPS12, Murf2, and 9S rRNA,
393 respectively. 1390 and 1400 are abbreviations for the cytosolic HGPRT isoforms Tb927.10.1390
394 and Tb927.10.1400, respectively. Tub is tubulin. Other short names are standard.
395

396 **Analysis of recombinant REH2 *in vitro***
397
398 The conserved predicted catalytic domains in REH2, the unwinding activity of pulldowns of
399 REH2 and ^{H2}F1 from extracts, and the loss of this activity in the pulldowns after mutating catalytic
400 amino acids in REH2, indicate that REH2 in the context of its native subcomplex functions as an RNA
401 helicase (3, 4, 23). However, the unwinding activity of the isolated REH2 has not been formally
402 established. We have now generated a his-tagged recombinant full-length rREH2 polypeptide (240
403 kDa) without its mitochondrial leader sequence (see the methods section) that supports robust ATP-
404 dependent unwinding of a synthetic dsRNA substrate *in vitro.* This polypeptide is largely intact in
405 most preparations (Fig. 6A). The dsRNA substrate in our assay is a mimic of the native A6 editing
406 system formed by pre-annealing of a 3' fragment of the pre-mRNA A6 with a cognate gRNA.
407 The synthetic A6 mRNA/gRNA pair supports a full round of U-deletion editing in an *in vitro*
408 assay with cell extracts and purified RECC enzyme (27, 28). The unwinding activity of the
409 recombinant enzyme increased in a titration with increasing concentrations of rREH2, and also in a
410 time course up to 30 min when most of the annealed radiolabeled RNA was unwound (Figs. 6B-C).
411 An upshift of radiolabeled RNA in a ribonucleoprotein complex at the highest tested concentrations of
412 rREH2 in the titration may be due to the known RNA binding activity of the native REH2 established
413 by UV crosslinking (5, 23). The radiolabeled strand alone (gRNA) and in heat-treated controls of the

414 dsRNA substrate exhibit the same gel mobility as the helicase-unwound gRNA (Figs. 6C-D). In
415 summary, the isolated 240 kDa recombinant REH2 is a *bona fide* RNA helicase enzyme *in vitro*, and
416 further supports the idea that REH2 may remodel RNA or its RNPs in editing.
417
418 **Figure 6. Recombinant rREH2 is a catalytically active RNA helicase. (A)** Purified rREH2[30-
419 2167] samples in a denaturing gel stained with Coomassie. NTA-Ni elution fractions 1-to-3 are
420 shown with molecular size markers (kDa). **(B)** Unwinding assays in 10 μL reaction mixtures with
421 increasing concentrations of rREH2[30-2167] +/- ATP. An RNP complex (RNP) forms at the
422 highest enzyme concentration tested; **(C)** Unwinding assays at increasing incubation times with
423 rREH2[30-2167] +/- ATP using the standard reaction mixture described in the material and
424 methods section. The standard reaction used a molar excess of enzyme over substrate. The
425 dsRNA (ds) was assembled by pre-annealing of synthetic transcript that mimics a 3' fragment of
426 the *T. brucei* A6 pre-edited mRNA and a radiolabeled cognate guide RNA (27). Radiolabeled
427 unwound ssRNA (ss) is indicated. Input dsRNA was heat denatured (Δ) as control. **(D)**
428 Additional controls showing that the starting radiolabeled ssRNA used to generate the dsRNA
429 substrate in the assay and the unwound radiolabeled ssRNA in the heat-denatured (Δ) dsRNA
430 (in panel B) have the same gel mobility.
431

432 Discussion

433
434 In the current study, we examined over 20 constructs of REH2 and ^{H2}F1 (Tables 1 and 2) to
435 identify features in these editing proteins that impact the stability of REH2, the assembly of the
436 REH2C RNP, and its RNA-mediated coupling with other components of the RNA editing holoenzyme
437 (or RNA holo-editosome). We also formally established that the isolated REH2 is a bona fide RNA
438 helicase enzyme.

439

440 The mRNA editing *trans* factors core enzyme RECC and accessory RESC and REH2C
441 exhibit transient and stable contacts with each other via RNA. Variants of RECC and the RESC
442 modules, GRBC and REMC, are also emerging in studies by different labs (reviewed in 1). These
443 variants imply a dynamic nature of holo-editosomes that may be important in editing control and
444 needs further characterization. The helicase complex REH2C exhibits transient and stable contacts
445 with variants of RESC that minimally differ in the relative content of MRB3010 (in the GRBC module).
446 This study focused on stable interactions by REH2C that can be readily examined. Prior studies *in*
447 *vivo* showed that inactivating mutations in the helicase ATP binding site or the dsRBD2 domain
448 dissociate REH2 from mRNA and RESC components, suggesting a general helicase detachment
449 from the editing apparatus (3). ^{H2}F1 RNAi dissociates the helicase from canonical proteins in the
450 RESC modules. RNAi knockdown of either ^{H2}F1 or REH2 also inhibited the editing associated with a
451 RESC variant that is particularly active and transiently interacts with REH2C (3, 4). These and other
452 observations indicate that transient and stable contacts in dynamic holo-editosomes including
453 those involving REH2C are important.
454 A systematic mutagenesis in the current study identified features affecting the assembly of
455 the REH2C RNP, or its association with other editing components *in vivo.*
456

457 **REH2 mutants *in vivo***
458
459 The NTR truncations examined here (>1000 residues each), ΔN and ΔNds, caused a major
460 loss in ^{H2}F1 binding and RNA-mediated association with GAP1. The only difference between the ΔN
461 and ΔNds constructs is that the latter lacks the ~70 amino acid dsRBD2 domain. As mentioned
462 above, the dsRBD2 promotes the addition of REH2 into holo-editosomes (3). Also, the dsRBD2 in the
463 related helicase MLE in flies may provide a major RNA-binding surface (29, 30). The tested
464 truncations suggest that other N-terminal features besides dsRBD2, may contribute to normal

465 interactions by REH2 *in vivo*. These truncations may also introduce topological changes that alter the
466 normal REH2 interactions but did not prevent localization of the constructs in enriched-mitochondrial
467 extracts (S2 Fig.). Conformational changes were proposed to modulate interactions by other
468 eukayotic DExH/RHA helicases (18, 31). Overall, the tested NTR truncations may indicate the
469 presence of unidentified protein features or global changes in conformation that affect the REH2
470 interactions. Further studies will be needed to resolve these possibilities. However, relatively short
471 CTR truncations and point mutations that affected the REH2 interactions with other editing
472 components are less likely to cause major conformation changes in REH2.
473
474 We have speculated that the conserved OB fold in DExH/RHA subfamily helicases may
475 share functional residues in kinetoplastid RNA editing and other RNA processes (14). Our examined
476 C-terminal truncations included most of the CTR (260 residues in ΔOB) or elements beyond the
477 OB fold that may be specific of REH2 (123 residues in ΔAOB). We examined R2023 in REH2
478 that corresponds to R704 in helicase Prp43p in yeast spliceosomes (16) (S3 Fig.). R2023
479 should be located in a critical loop, β4-β5, in the REH2 OB fold. In yeast, R704 is poised to
480 interact with the RNA substrate entering the helicase cavity, and mutation of this residue inhibits
481 the RNA binding and RNA-mediated activation of Prp43p (16). We also examined R1979 in
482 REH2, which is not conserved in Prp43p. In trypanosomes, the R2023A substitution had a
483 moderate effect on the stable RNA-mediated association of REH2C with GAP1. However,
484 R1979A did not evidently affect this interaction. Neither R1979A or R2023A seem to
485 significantly affect the REH2 direct interaction with ^{H2}F1.
486 Similarly, H1998 and R1999 in REH2 were compared to the equivalent H1032 and
487 K1033 positions in the RNA helicase MLE in flies. The later residues in MLE bind specific
488 uridylates in U-rich roX boxes of the cognate roX RNA. H1032 and K1033 are also needed for
489 the chromosomal localization of MLE in the *Drosophila* dosage compensation complex (18). The

490 H1998E substitution had a moderate effect on the REH2 association with GAP1 but had little or
491 no effect on the interaction with ^{H2}F1. In contrast, the adjacent substitution R1999E affected
492 both the direct REH2 interaction with ^{H2}F1 and the RNA-based REH2 association with GAP1.
493 These results are consistent with the idea that ^{H2}F1 is an adaptor protein of REH2 (4), and that
494 structure-function correlations may be tractable to specific conserved amino acids in REH2 and
495 related helicases in highly-diverged species (14). This is also in line with the idea that the OB
496 fold in DExH/RHA helicases, including REH2, is a conserved regulatory domain.
497

498 **^{H2}F1 mutants *in vivo***
499
500 ^{H2}F1 has eight predicted C2H2 Znf domains that cover over ~45% of the polypeptide
501 sequence. Apart from the Znf domains, ^{H2}F1 has no evident sequence or structural conservation
502 outside of the kinetoplastids. ^{H2}F1is an adaptor protein that brings the REH2 to the editing machinery
503 (4) and it also stabilizes REH2. That is, the induced downregulation of ^{H2}F1 caused fragmentation of
504 REH2 (4), and we showed here that the converse upregulation of ^{H2}F1 increased the REH2 level *in*
505 *vivo*. ^{H2}F1 may require most of its zinc fingers to stabilize REH2 because loss of the core structure or
506 positive charge in individual fingers compromised this function. It is feasible that the stabilizing effect
507 of ^{H2}F1 involves substantial changes in the helicase conformation and coordination of its zinc fingers.
508 Notably, all examined ^{H2}F1 substitution-mutants were able to associate with REH2, GAP1, and REL1.
509 This suggested that the basic fold or positive charge of the fingers is not essential for the ^{H2}F1
510 association with other editing components. However, N- or C-terminal truncation of nearly half the
511 size of ^{H2}F1 hampered its normal interactions with the examined editing components. The ^{H2}F1 ΔN
512 accumulated in enriched-mitochondrial extracts but the ^{H2}F1 ΔC localization in mitochondria seemed
513 relatively compromised. Somehow the C-terminal truncation was particularly deleterious to ^{H2}F1.
514 Additional studies are needed to pinpoint specific determinants for ^{H2}F1 direct binding to REH2 or its
515 RNA-mediated contacts with other components.

516 Besides the REH2•^{H2}F1 system, other DExH/RHA helicase•Znf protein pairs have been
517 characterized (14). In the DXH30•ZAP system in antivirus protection in humans, the antiviral protein
518 ZAP has four Znf motifs that participate in viral RNA recognition (32, 33). All four fingers lie on a
519 positively charged surface in a crystal structure of ZAP (25) and mutation of basic residues in the
520 fingers inhibited the ZAP antiviral function (33). The ZAP studies imply that stabilization of REH2 by
521 ^{H2}F1 could involve a precise topology of its zinc fingers, and that the ^{H2}F1 fingers may participate in
522 RNA binding. Notably, recombinant ZAP is multimeric (25). If ^{H2}F1 dimerizes, a single REH2C RNP
523 would include 16 zinc fingers. The co-purification of tagged and endogenous ^{H2}F1 from RNase-
524 treated extracts imply direct protein contacts between the ^{H2}F1 copies (S7 Fig.). However, analyses
525 of recombinant ^{H2}F1 WT and mutants are necessary to establish the potential of ^{H2}F1 to multimerize
526 and bind RNA, and to define the role of its fingers. The RNA content in pulldowns of the ^{H2}F1 Znf4
527 variant with four R/K>A substitutions suggested minimal changes in association with target RNAs in
528 mitochondria but a significance loss in non-specific contacts with unrelated transcripts. This suggests
529 that subtle changes in RNA affinity are more likely to affect weak non-specific RNA contacts. The
530 general loss of transcripts examined in the pulldowns of the tested ^{H2}F1 fragments also suggests that
531 efficient RNA association by the REH2C complex *in vivo* involves a full array of zinc fingers in ^{H2}F1.
532 We note that the transcripts examined may associate with either ^{H2}F1, REH2 or both proteins in the
533 native REH2C RNP.
534

535 **REH2 may function as an RNA helicase in kinetoplastid RNA editing**
536
537 Prior studies suggested that REH2 is a functional helicase in RNA editing. REH2 pulldowns
538 from GAP1-depleted extracts exhibit RNA unwinding activity (4), and the mutation of catalytic
539 residues in the predicted RecA1 domain inhibits the unwinding activity in pulldowns of REH2 (23).
540 We have now established that the isolated full-length recombinant REH2 (240 kda) is a *bona fide*
541 RNA helicase enzyme. This further indicates that REH2, the only DExH/RHA helicase in kinetoplastid

542 holo-editosomes provides an ATP-dependent unwinding activity in RNA editing. Additional studies
543 are needed to determine if ^{H2}F1 affects the activity of REH2. Besides REH2, the editing apparatus
544 also requires the DEAD-box RNA helicase REH1 (12, 13). REH1 is not part of the RNPs studied here
545 and seems to lack a direct binding partner. A transient RNA-mediate interaction of REH1 with
546 other editing proteins has been detected (23, 34). REH1 and REH2 are functionally different.
547 REH2 is needed for editing within single blocks, including the first "initiating" block (3). In
548 contrast, REH1 is needed for editing of two or more blocks (i.e., by overlapping gRNAs) but has
549 no effect on the first block, suggesting a role in gRNA exchange (13). Both RNA helicases may
550 promote critical remodeling of RNA or RNP structure. Our ongoing RNA-seq analyses may
551 provide additional functional insights concerning REH2C (Kumar et al., unpublished).
552

553 **Possible roles of editing complex variants**
554
555 The editing apparatus much like the splicing and transcription molecular machines may
556 exhibit dynamic phases of assembly and function. The RECC enzyme has multiple isoforms that
557 include several RNase III (RIII)-like protein subunits. These RIII proteins have the potential to
558 form a large number of binary combinatorial that could modulate substrate recognition (35-37).
559 Also, natural GRBC and REMC isoforms and genetically-induced changes in their protein/RNA
560 organization are emerging. A recurring theme is the variable interaction between the essential
561 GAP1/2 heterotetramer in all editing involving GRBC-bound gRNAs, and MRB3010 (GRBC6)
562 that participates in early editing (1, 6, 38). A controlled interaction of the GAP1/2 tetramer with
563 MRB3010 may modulate editing. For example, GRBC variants in pulldowns of MRB3010 or
564 REH2 differ in relative content of MRB3010 and editing level in associated mRNAs (3, 5).
565 However, RNAi of REH2 or ^{H2}F1 caused a reduced editing in mRNAs in the MRB3010 pulldowns
566 (3, 4). REH2 and ^{H2}F1 features, including those examined here, may affect specific steps in the
567 editing mechanism and we are currently addressing this.

568

569 # Materials and methods
570

571 ## Cell Culture
572

573 *T. brucei* Lister strain 427 29-13 procyclic was grown axenically in log phase in SDM79
574 medium (39) and harvested at a cell density of 1–3x10^7 cells/mL. All transgenic cell lines were
575 induced with tetracycline at 1µg/mL. The REH2 WT-TAP and ^{H2}F1 RNAi cell lines that were
576 used as controls were generated in our lab (3, 4). We have seen that the TAP tag in REH2,
577 including the WT construct, seems to slow the growth of trypanosomes after several days of
578 culture (23). This and presumably incomplete cloning after transfection may account for the
579 uneven expression levels in extracts from independent subcultures. To partially control for this
580 issue, most plasmid constructs used to generate the current data figures were made to use
581 puromycin selection. Most transfections used tetracycline-screened HyClone Fetal Bovine
582 Serum (FBS) (SH30070.03T; GE Healthcare. This enabled a faster cell recovery after
583 transfection than with constructs using phleomycin selection that were originally used in cell
584 lines appearing somewhat less stable during subculture. Regardless of this issue, independent
585 analyses of protein associations were consistent with either puromycin or phleomycin
586 constructs.

587

588 ## DNA constructs
589

590 All overexpression and RNAi studies used inducible plasmid constructs. The constructs
591 for ^{H2}F1 RNAi and the REH2 dsRBD2 mutant K1078A/A1086D were previously reported (3, 4).
592 N-terminal deletion constructs for REH2 (ΔN and ΔNds) and ^{H2}F1 (ΔN) were prepared using the
593 In-Fusion® HD Cloning Kit (639648; Clontech). Two PCR amplicons were prepared in each
594 case using CloneAmp™ HiFi PCR Premix (638500; Clontech) and were then gel-eluted using

595 NucleoSpin® Gel and PCR Clean-up (740609.10; Clontech). One amplicon encodes the first 34
596 amino acids of REH2 (primers: F-1503, R-1522), including the predicted REH2 mitochondrial
597 leader sequence (REH2-MLS) (23), that was used for all N-deletion constructs. The other
598 amplicon included the remaining relevant gene fragment sequence: 3070-6501 bases (REH2
599 ΔN), 3280-6501 bases (REH2 ΔNds), or 766-1572 bases (^{H2}F1 ΔN). Three-piece in-fusion
600 reactions were performed to join the two amplicons and pLEW79-ada-TAP plasmid linearized at
601 *XhoI* and *BamHI* (40). The PCR primers (S1 Table) included 5' and 3' terminal homology (15
602 bases) to enable the recombination-based fusion between the amplicons and the plasmid DNA.
603 The REH2 (ΔAOB and ΔOB) and ^{H2}F1 ΔC deletion constructs are also recombination-based
604 fusions of the amplified relevant gene fragment with linearized plasmid DNA. The REH2
605 constructs R2023A, H1998E, R1999E and H1998E/R1999E, and the ^{H2}F1 construct Znf5 C>A
606 were created by site-directed mutagenesis in inverse-PCR reactions of the pLEW79-ada-TAP
607 WT plasmid as the template. pLEW79-ada-TAP was modified from the original pLEW79-TAP
608 (40, 41). The resulting linearized mutant constructs were circularized using the In-Fusion HD
609 Cloning Kit. Other ^{H2}F1 constructs used synthetic gBlock gene fragments (IDT) with mutations.
610 N-terminal fragments of ^{H2}F1 (Znf1, Znf2 and Znf3 R/K>A single finger mutants) replaced the
611 corresponding sequence in the ^{H2}F1 WT construct after digestion with *XhoI* and the internal
612 *ApaI* site in ^{H2}F1. A C-terminal fragment of ^{H2}F1 to generate Znf4R/K>A or Znf5 R/K>A replaced
613 a corresponding sequence in the ^{H2}F1 WT construct after digestion with *ApaI* and *BamH1*. The
614 ^{H2}F1 WT construct was made by ligation of an amplicon with the full open reading frame into
615 pLEW79-ada-TAP plasmid linearized at *XhoI* and *BamHI.* All constructs were confirmed by DNA
616 sequencing, linearized with *NotI*, and transfected in trypanosomes (39).
617

618 **Western Blots and Radioactivity Assays**
619

620 Western blots of REH2, ^{H2}F1 and ^{H2}F2 (subunits of REH2C), GAP1 (alias GRBC2;
621 subunit of GRBC) and A2 (alias MP42; subunit of RECC) were performed as reported (4, 23).
622 Western blots of the GAP1/GAP2 (alias GRBC2/GRBC1) paralogs simultaneously, and of
623 MRB8170 and MRB6070 (subunits of REMC and MRB6070/1590 assemblies, respectively),
624 were performed as previously described (42, 43). GAP1 alone was examined in the main data
625 figures. Both GAP1/GAP2 were examined in S1 and S5 figures. Peroxidase Anti-peroxidase
626 antibody (P1291; Sigma) diluted to 1:200 (v/v) was used to detect the TAP-tag. EF-1 α1
627 antibody (sc-21758; Santa Cruz Biot) diluted to 1:200 (v/v) was used as a cytosolic marker.
628 Protein quantitative analyses using Amersham ECL™ western blot detection reagents were
629 performed in an Amersham Imager 600. RNA ligases in the RECC enzyme were radiolabeled
630 by self-adenylation directly on the beads in IgG pulldowns (44). Unwinding assays of REH2
631 used reported conditions with a few modifications (4) and full-length recombinant His-REH2.
632 The dsRNA substrate in these assays used an A6 mRNA/gRNA pair (23). The A6 pair mimics
633 the endogenous ATPase subunit 6 substrate. The gRNA was transcribed with RNA T7
634 polymerase from an amplicon (S1 Table) after *DraI* restriction digestion and gel purification of
635 the product. The 61-nt gRNA was 5'-labelled with γ^{32}P-ATP using T4 Polynucleotide kinase. The
636 62-nt mRNA was synthetic (IDT). A mix with 3 pmoles of labelled gRNA and 15 pmoles of
637 mRNA was heated at 95° C for 3 min, and then immediately incubated for 30 min at room
638 temperature in the annealing buffer (10 mM MOPS pH 6.5, 1 mM EDTA, and 50 mM KCl). The
639 annealed RNA hybrids were isolated from native 12% PAGE run at 4 ˚C at 50 V for 120 min in
640 0.5x Tris-borate-EDTA buffer. Standard 10 μL reaction mixtures in unwinding buffer (40 mM
641 Tris-Cl pH 8.0, 0.5 mM $MgCl^2$, 0.01% Nonidet P-40, and 2 mM DTT) were incubated for 30 min
642 at 19 °C with 20 cps of hybrid (~20 fmoles) and 3 μg of recombinant REH2 (~12 pmoles).
643 Variations to the standard assay including in the concentration of REH2 or the reaction time are
644 indicated in the text. All assays contained 100 fmoles of unlabeled gRNA as competitor to

645 prevent re-annealing of unwound γ^{32}P-gRNA. The assays were stopped with an equal volume of
646 2x helicase reaction stop buffer (50 mM EDTA, 1% SDS, 0.1% bromophenol blue, 0.1% xylene
647 cyanol, and 20% glycerol) and kept on ice for 5 min. The assays in Fig. 6B were also treated
648 with 0.4U of proteinase K (P8107S; NEB), 25 mM EDTA and 0.5% SDS at 22° C for 30 min.
649 The entire reaction was loaded onto a native 12% PAGE and resolved at 25 V for 120 min at
650 4°C.
651

652 **Cell extracts and purification of protein and RNA from IgG pulldowns**
653
654 Whole cell extracts as well as mitochondria-enriched (mini-mito) extracts were used in
655 this study. Whole-cell extracts were generated by incubation of cell pellets in MRB-Triton buffer
656 (25 mM Tris-Cl pH 8.0, 10 mM MgOAC, 1 mM EDTA, 10 mM KCl, 5% glycerol, 0.5% Triton X-
657 100) at 4 °C for 45 minutes followed by centrifugation at 15,000g for 30 minutes. Mitochondria-
658 enriched extracts were prepared using a simplified protocol similar to others reported earlier (2,
659 45). Namely, cell pellets were resuspended into hypotonic DTE buffer (1 mM Tris-HCl pH 8.0, 1
660 mM EDTA pH 8.0) supplemented with protease inhibitors and disrupted in a Dounce
661 homogenizer. The suspension was passed through a 26-gauge needle as originally described
662 (46). The enriched mitochondrial vesicles were spun down and the cytosolic content in the
663 supernatant discarded. This step improved the recovery of intact REH2 compared to whole-cell
664 extracts. REH2 is more prone to fragmentation than other proteins examined in this study. The
665 following steps were also as in (46). The pellet was resuspended into STM buffer (0.25M
666 Sucrose, 20 mM Tris-HCl pH 8.0, 2 mM $MgCl_2$) supplemented with DNase I, RNase-free
667 (EN0523; Fisher Scientific). The reaction was stopped with one volume of STE buffer (0.25 M
668 Sucrose, 20 mM Tris-HCl pH 8.0, 2 mM EDTA pH 8.0). The enriched mitochondria were spun
669 down and washed in STE buffer. The pellet was resuspended into MRB-Triton buffer and
670 incubated in ice for 15 min. The suspension was spun down at 15,000g at 4 °C for 30 min. The

671 supernatant was collected and stored at -80 °C. In IgG pulldowns of the extracts, ectopically
672 expressed TAP-REH2 and TAP-^{H2}F1 were recovered as reported (4, 23) with some
673 modifications. Approximately 2 mg of protein was mixed with 1x SUPERase·In™ RNase
674 inhibitor (Invitrogen™) and incubated with Dynabeads IgG (11203D; Invitrogen™). The beads
675 were washed five times with 1ml of wash buffer (150 mM NaCl, 1 mM EDTA, 10 mM MgAOc,
676 0.1% NP-40, and 25 mM Tris pH 8.0). Protein was eluted from the beads with 15 μL of 1x SDS
677 loading buffer at 95 °C for 2 min. RNA was extracted by treating the beads with 4U proteinase K
678 (NEB) for 2 hrs at 55 °C, followed by phenol extraction and ethanol precipitation. For some
679 pulldowns, RNase A/T1 mix (EN0551; Fisher Scientific) was applied at 20 U/mg of protein both
680 in the input extract and again while bound to the beads.
681

682 **Quantitative RT-PCR**
683
684 Isolated RNA from the pulldowns or directly from input extracts was treated with DNase
685 I, RNase-free (EN0523; Thermo Scientific™) prior to cDNA synthesis with the iScript™ Reverse
686 Transcription Supermix (Bio-Rad) as described elsewhere (5). The amplifications mixtures (10
687 µl) used SsoAdvanced™ Universal SYBR® Green Supermix (Bio-Rad) and reported
688 oligonucleotides for unedited mRNAs, fully edited mRNA, and reference transcripts (47). Diluted
689 samples of the examined cDNA produced a single amplicon during linear amplification under
690 our conditions. The end-point amplicons described here have been gel-isolated, cloned and
691 confirmed by sequencing as previously described (5). Fold-enrichment of mitochondrial and
692 cytosolic transcripts in IgG pulldowns of tagged proteins (induced extracts), relative to a mock
693 pulldown (uninduced extract), was calculated as follows: Fold = $2^{[-ddCq]}$, where ddCq = Cq test
694 IP – Cq mock IP, as in (5). The relative value for each mutant construct was adjusted to the
695 amount of recovered tagged protein, and subsequently normalized to the tagged WT construct
696 (= 1). The plot in Fig. 5B was constructed using data from 3 independent biological replicate

697 experiments, including a total of six amplicons per data point (i.e., two technical replicate
698 amplicons per assay). Two of the independent experiments (including cultures +/- Tet for each
699 mutant) were performed concurrently. The third independent experiment (one set of cultures per
700 mutant +/- Tet) was conducted on a subsequent date. The replicate experiments showed a
701 consistent sample loading in the assays used in our plots. The examined mutant constructs
702 differed in the amount of non-specific association with Tubulin and other cytosolic transcripts
703 that are normally used as internal reference in antibody pulldowns using a common protein bait.
704 The raw Cq values of examined editing transcripts in the pulldowns and the plotted values after
705 normalization indicated a substantial loss of these transcripts in the truncated mutants.
706 qRT-PCR assays of input extract in S8 Fig. were normalized using the following equation: Ratio
707 (reference/target) = $2^{[Cq(ref) - Cq(target)]}$. This scores the relative difference between the reference
708 and target Cq values. The current plots of input extract used 18S rRNA as reference (S8 Fig.).
709 We obtained similar results with any of these cytosolic transcripts used as a reference: tubulin,
710 1400 or 1390 (Tb927.10.1400 or Tb927.10.1390, respectively).
711

712 **Homology modeling and bioinformatics analysis**
713
714 The multiple-sequence alignment of REH2 and MLE, and that of the ^{H2}F1 zinc finger
715 domains, was done with Clustal Omega (48). Formatting of the fingers alignment was done with
716 BOXSHADE version 3.21 (http:/www.ch.embnet.org/software/BOX_form.html). Sequence
717 alignment of Prp43p, REH2, and other helicases was done using the CDD tool in NCBI (49).
718 The structure-based searches of *T. brucei* REH2 used the program Phyre2 (20). The homology
719 model of REH2 derived from the structure of yeast Prp43p. The inset is a closer view of R2023 and the
720 surround region in the OB-fold. The molecular surface is colored by residue conservation. The image was
721 made using PyMOL version 2.2.

722

723 **Recombinant protein**

724

725 6xHis-REH2 (amino acid residues 30-2167) was amplified by PCR (S1 Table). The gel-
726 purified product was cloned into the NcoI and BamHI sites in the expression vector pET15b by
727 using the NEBuilder® HiFi DNA Assembly Master Mix (E262, NEB) and the appropriate primers.
728 The ligation reaction mixtures were transformed into chemically competent Omnimax cells from
729 ThermoFisher Scientific. Colonies with the correct insert were identified by single-colony PCR
730 and then amplified for plasmid purification. The sequence of the flanking vector region and the
731 insert was checked by DNA sequencing. The plasmid DNA was transformed into Rosetta2 DE3
732 cells (Novagen Inc.) and overexpressed in 4 L of Terrific Broth media by supplementing 2% (v/v)
733 ethanol and 2 mM $MgCl_2$ at 37 °C. Protein induction with 0.5 mM IPTG was done at a OD_{600} of
734 0.8, and the expression was continued for 22 hours at 16 °C. The cell pellet was stored at -80
735 °C overnight and was resuspended in lysis buffer (5 mL/g of cell pellet) of 50 mM Tris-HCl pH
736 8.0, 250 mM NaCl, 1 mM EDTA, and 1 mM DTT along with 10 µg of RNase-free DNase and 15
737 mg of hen egg white lysozyme. The cells were lysed in an Emulsiflex hydraulic press. The cell
738 debris was pelleted at 39,200 x g for 30 minutes at 4 °C. The supernatant with 6xHis-REH2 was
739 batch attached to equilibrated Qiagen Ni-NTA Agarose at 4 °C for 16 hrs. The helicase was
740 eluted with 50 mM Tris-HCl pH 8.0, 300 mM NaCl, 1 mM DDT, and 250 mM imidazole. The first
741 elution of the purification was dialyzed into unwinding assay buffer. This material was tested for
742 the presence of the recombinant protein in 6% SDS-PAGE stained with Commassie blue,
743 western blots and antibody pulldowns, and for activity in dsRNA unwinding activity assays *in*
744 *vitro*.

745

746 **Acknowledgements**

747

748 We thank the Read lab for their gift of antibodies against GAP1, TbRGG2 (alias RGG2),

749 MRB6070, MRB8170, and ^{H2}F2. The Afasizhev lab kindly provided antibodies that react against
750 the GAP1/GAP2 paralogs (alias GRBC2/GRBC1) simultaneously. We also thank the Stuart lab
751 for providing the antibodies against A2 (alias MP42). Amna Mushtaq provided detailed
752 comments on the manuscript. Jana Gomez, Elizabeth Alvarez and Melissa Yang helped with
753 the preparation of figures.

754

755 # References

756

757 1. Cruz-Reyes J, Mooers BHM, Doharey PK, Meehan J, Gulati S. Dynamic RNA
758 holoeditosomes with subcomplex variants: Insights into the control of trypanosome editing.
759 WIREs RNA. 2018;e1502.
760 2. Koslowsky DJ, Sun Y, Hindenach J, Theisen T, Lucas J. The insect-phase gRNA
761 transcriptome in Trypanosoma brucei. Nucleic acids research. 2013.
762 3. Madina BR, Kumar V, Mooers BH, Cruz-Reyes J. Native Variants of the MRB1 Complex
763 Exhibit Specialized Functions in Kinetoplastid RNA Editing. PloS one. 2015;10(4):e0123441.
764 4. Kumar V, Madina BR, Gulati S, Vashisht AA, Kanyumbu C, Pieters B, et al. REH2C
765 Helicase and GRBC Subcomplexes May Base Pair through mRNA and Small Guide RNA in
766 Kinetoplastid Editosomes. J Biol Chem. 2016;291(11):5753-64.
767 5. Madina BR, Kumar V, Metz R, Mooers BH, Bundschuh R, Cruz-Reyes J. Native
768 mitochondrial RNA-binding complexes in kinetoplastid RNA editing differ in guide RNA
769 composition. RNA. 2014;20(7):1142-52.
770 6. Aphasizheva I, Zhang L, Wang X, Kaake RM, Huang L, Monti S, et al. RNA binding and
771 core complexes constitute the U-insertion/deletion editosome. Mol Cell Biol. 2014;34(23):4329-
772 42.
773 7. Huang Z, Faktorova D, Krizova A, Kafkova L, Read LK, Lukes J, et al. Integrity of the
774 core mitochondrial RNA-binding complex 1 is vital for trypanosome RNA editing. RNA. 2015.
775 8. McAdams NM, Simpson RM, Chen R, Sun Y, Read LK. MRB7260 is essential for
776 productive protein-RNA interactions within the RNA editing substrate binding complex during
777 trypanosome RNA editing. RNA. 2018;24(4):540-56.
778 9. Simpson RM, Bruno AE, Bard JE, Buck MJ, Read LK. High-throughput sequencing of
779 partially edited trypanosome mRNAs reveals barriers to editing progression and evidence for
780 alternative editing. RNA. 2016;22(5):677-95.
781 10. Simpson RM, Bruno AE, Chen R, Lott K, Tylec BL, Bard JE, et al. Trypanosome RNA
782 Editing Mediator Complex proteins have distinct functions in gRNA utilization. Nucleic acids
783 research. 2017;45(13):7965-83.
784 11. Shaw PL, McAdams NM, Hast MA, Ammerman ML, Read LK, Schumacher MA.
785 Structures of the T. brucei kRNA editing factor MRB1590 reveal unique RNA-binding pore motif
786 contained within an ABC-ATPase fold. Nucleic acids research. 2015;43(14):7096-109.
787 12. Missel A, Souza AE, Norskau G, Goringer HU. Disruption of a gene encoding a novel
788 mitochondrial DEAD-box protein in Trypanosoma brucei affects edited mRNAs. Mol Cell Biol.
789 1997;17(9):4895-903.

790 13. Li F, Herrera J, Zhou S, Maslov DA, Simpson L. Trypanosome REH1 is an RNA helicase
791 involved with the 3'-5' polarity of multiple gRNA-guided uridine insertion/deletion RNA editing.
792 Proc Natl Acad Sci U S A. 2011;108(9):3542-7.
793 14. Cruz-Reyes J, Mooers BH, Abu-Adas Z, Kumar V, Gulati S. DEAH-RHA helicase•Znf
794 cofactor systems in kinetoplastid RNA editing and evolutionarily distant RNA processes. RNA
795 Dis. 2016;3(2):e1336.
796 15. Jarmoskaite I, Russell R. RNA helicase proteins as chaperones and remodelers. Annu
797 Rev Biochem. 2014;83:697-725.
798 16. Walbott H, Mouffok S, Capeyrou R, Lebaron S, Humbert O, van Tilbeurgh H, et al.
799 Prp43p contains a processive helicase structural architecture with a specific regulatory domain.
800 EMBO J. 2010;29(13):2194-204.
801 17. Robert-Paganin J, Rety S, Leulliot N. Regulation of DEAH/RHA helicases by G-patch
802 proteins. Biomed Res Int. 2015;2015:931857.
803 18. Prabu JR, Muller M, Thomae AW, Schussler S, Bonneau F, Becker PB, et al. Structure
804 of the RNA Helicase MLE Reveals the Molecular Mechanisms for Uridine Specificity and RNA-
805 ATP Coupling. Mol Cell. 2015;60(3):487-99.
806 19. Dhote V, Sweeney TR, Kim N, Hellen CU, Pestova TV. Roles of individual domains in
807 the function of DHX29, an essential factor required for translation of structured mammalian
808 mRNAs. Proc Natl Acad Sci U S A. 2012;109(46):E3150-9.
809 20. Kelley LA, Mezulis S, Yates CM, Wass MN, Sternberg MJ. The Phyre2 web portal for
810 protein modeling, prediction and analysis. Nat Protoc. 2015;10(6):845-58.
811 21. Cruz-Reyes J. MBHM, Kumar K., Doharey P.K., Meehan J., Chaparro L. Control
812 Mechanisms of the Holo-Editosome in Trypanosomes. In: J C-R, M G, editors. RNA Metabolism
813 in Mitochondria. Nucleic Acids and Molecular Biology. 34: Springer, Cham; 2018.
814 22. Jankowsky E. RNA helicases at work: binding and rearranging. Trends in biochemical
815 sciences. 2011;36(1):19-29.
816 23. Hernandez A, Madina BR, Ro K, Wohlschlegel JA, Willard B, Kinter MT, et al. REH2
817 RNA helicase in kinetoplastid mitochondria: ribonucleoprotein complexes and essential motifs
818 for unwinding and guide RNA (gRNA) binding. J Biol Chem. 2010;285(2):1220-8.
819 24. Segal DJ, Crotty JW, Bhakta MS, Barbas CF, 3rd, Horton NC. Structure of Aart, a
820 designed six-finger zinc finger peptide, bound to DNA. J Mol Biol. 2006;363(2):405-21.
821 25. Chen S, Xu Y, Zhang K, Wang X, Sun J, Gao G, et al. Structure of N-terminal domain of
822 ZAP indicates how a zinc-finger protein recognizes complex RNA. Nat Struct Mol Biol.
823 2012;19(4):430-5.
824 26. Klug A. The discovery of zinc fingers and their development for practical applications in
825 gene regulation and genome manipulation. Q Rev Biophys. 2010;43(1):1-21.
826 27. Seiwert SD, Heidmann S, Stuart K. Direct visualization of uridylate deletion in vitro
827 suggests a mechanism for kinetoplastid RNA editing. Cell. 1996;84(6):831-41.
828 28. Rusche LN, Cruz-Reyes J, Piller KJ, Sollner-Webb B. Purification of a functional
829 enzymatic editing complex from Trypanosoma brucei mitochondria. EMBO J. 1997;16(13):4069-
830 81.
831 29. Izzo A, Regnard C, Morales V, Kremmer E, Becker PB. Structure-function analysis of the
832 RNA helicase maleless. Nucleic acids research. 2008;36(3):950-62.
833 30. Masliah G, Barraud P, Allain FH. RNA recognition by double-stranded RNA binding
834 domains: a matter of shape and sequence. Cell Mol Life Sci. 2013;70(11):1875-95.
835 31. Christian H, Hofele RV, Urlaub H, Ficner R. Insights into the activation of the helicase
836 Prp43 by biochemical studies and structural mass spectrometry. Nucleic acids research.
837 2014;42(2):1162-79.
838 32. Ye P, Liu S, Zhu Y, Chen G, Gao G. DEXH-Box protein DHX30 is required for optimal
839 function of the zinc-finger antiviral protein. Protein & cell. 2010;1(10):956-64.

840 33. Guo X, Carroll JW, Macdonald MR, Goff SP, Gao G. The zinc finger antiviral protein
841 directly binds to specific viral mRNAs through the CCCH zinc finger motifs. J Virol.
842 2004;78(23):12781-7.
843 34. Kruse E, Voigt C, Leeder WM, Goringer HU. RNA helicases involved in U-
844 insertion/deletion-type RNA editing. Biochimica et biophysica acta. 2013;1829(8):835-41.
845 35. Carnes J, Soares CZ, Wickham C, Stuart K. Endonuclease associations with three
846 distinct editosomes in Trypanosoma brucei. J Biol Chem. 2011;286(22):19320-30.
847 36. McDermott SM, Luo J, Carnes J, Ranish JA, Stuart K. The Architecture of Trypanosoma
848 brucei editosomes. Proc Natl Acad Sci U S A. 2016;113(42):E6476-E85.
849 37. Carnes J, McDermott S, Anupama A, Oliver BG, Sather DN, Stuart K. In vivo cleavage
850 specificity of Trypanosoma brucei editosome endonucleases. Nucleic acids research.
851 2017;45(8):4667-86.
852 38. Ammerman ML, Hashimi H, Novotna L, Cicova Z, McEvoy SM, Lukes J, et al. MRB3010
853 is a core component of the MRB1 complex that facilitates an early step of the kinetoplastid RNA
854 editing process. RNA. 2011;17(5):865-77.
855 39. Wirtz E, Leal S, Ochatt C, Cross GA. A tightly regulated inducible expression system for
856 conditional gene knock-outs and dominant-negative genetics in Trypanosoma brucei. Molecular
857 and biochemical parasitology. 1999;99(1):89-101.
858 40. Hernandez A, Panigrahi A, Cifuentes-Rojas C, Sacharidou A, Stuart K, Cruz-Reyes J.
859 Determinants for association and guide RNA-directed endonuclease cleavage by purified RNA
860 editing complexes from Trypanosoma brucei. J Mol Biol. 2008;381(1):35-48.
861 41. Panigrahi AK, Schnaufer A, Ernst NL, Wang B, Carmean N, Salavati R, et al.
862 Identification of novel components of Trypanosoma brucei editosomes. RNA. 2003;9(4):484-92.
863 42. Ammerman ML, Downey KM, Hashimi H, Fisk JC, Tomasello DL, Faktorova D, et al.
864 Architecture of the trypanosome RNA editing accessory complex, MRB1. Nucleic acids
865 research. 2012;40(12):5637-50.
866 43. Weng J, Aphasizheva I, Etheridge RD, Huang L, Wang X, Falick AM, et al. Guide RNA-
867 binding complex from mitochondria of trypanosomatids. Mol Cell. 2008;32(2):198-209.
868 44. Sabatini R, Hajduk SL. RNA ligase and its involvement in guide RNA/mRNA chimera
869 formation. Evidence for a cleavage-ligation mechanism of Trypanosoma brucei mRNA editing. J
870 Biol Chem. 1995;270(13):7233-40.
871 45. Hashimi H, Zikova A, Panigrahi AK, Stuart KD, Lukes J. TbRGG1, an essential protein
872 involved in kinetoplastid RNA metabolism that is associated with a novel multiprotein complex.
873 RNA. 2008;14(5):970-80.
874 46. Harris ME, Hajduk SL. Kinetoplastid RNA editing: in vitro formation of cytochrome b
875 gRNA-mRNA chimeras from synthetic substrate RNAs. Cell. 1992;68(6):1091-9.
876 47. Carnes J, Stuart KD. Uridine insertion/deletion editing activities. Methods in enzymology.
877 2007;424:25-54.
878 48. Sievers F, Higgins DG. Clustal Omega, accurate alignment of very large numbers of
879 sequences. Methods Mol Biol. 2014;1079:105-16.
880 49. Marchler-Bauer A, Derbyshire MK, Gonzales NR, Lu S, Chitsaz F, Geer LY, et al. CDD:
881 NCBI's conserved domain database. Nucleic acids research. 2015;43(Database issue):D222-6.
882

883

884 # Supporting information

885

886 **S1 Figure. Western blot analyses of RESC associated proteins in antibody pulldowns of**

887 **REH2 and MRB3010**. Immunoprecipitations (IP) from extract with specific antibodies against
888 REH2, MRB3010 or CoxI (mock). **(A)** Western blot analyses examined for the presence of
889 REH2, MRB8170 and MRB6070 proteins. These are markers of REH2C, REMC and a
890 MRB6070/MRB1590-containing subcomplex that associates with RESC, respectively. Extract
891 (Ext) used in the IPs and size markers in kDa (M) are indicated. **(B)** Western blot analyses as in
892 A examining REH2, the GAP1/GAP2 paralogs, and MRB6070. We note that proteins in the IPs
893 are often upshifted relative to the control extract lane. The cause of this upshift is unclear to us
894 but it may be a slight effect on the proteins migration due to the presence of IgG in those
895 samples. IgG in the pulldown lanes is indicated.
896
897 **S2 Figure. Western blot analyses of ectopically-expressed TAP constructs in whole-cell**
898 **and enriched-mitochondrial extracts**. Large-truncation constructs were compared in whole-
899 cell (WC) and enriched-mitochondrial (aka Mini-Mito "MM" extract): (A) REH2-ΔN, (B) REH2-
900 ΔNds, (C) ^{H2}F1-ΔN, and (D) ^{H2}F1-ΔC. Western blots of the tag in these constructs (TAP) and the
901 cytosolic marker eEF-1 indicate a partial enrichment of the constructs in the mini-mito extract.
902
903 **S3 Figure. The OB-fold in yeast helicase Prp43p (crystal structure pdb: 2XAU_B) and *T.***
904 ***brucei* REH2**. (A) Sequence alignment of Prp43p, REH2, and other DExH/RHA helicases. The
905 sequences were aligned using the CDD tool in NCBI. The residue R1979 in REH2 is not
906 conserved in the aligned sequences but the basic amino acid at position 2023 in REH2 (K704 in
907 Prp43p) is conserved. Secondary structure elements are indicated: α-helix (cylinders) and β-
908 strand (arrows). (B) homology model of R2023 in REH2 using the OB fold in Prp43p as a
909 template.
910
911 **S4 Figure. Multi-sequence alignment of a C-terminal segment in *T. brucei* REH2 and**
912 ***Drosophila* MLE DExH/RHA RNA helicases**. The alignment was generated with Clustal

913 Omega (48). Boxes were inserted manually to improve the match between the MLE and REH2
914 residues. Note that H1032, K1033 and T1034 (in red), which make U-specific contacts in MLE,
915 are aligned with H1998, R1999 and T2000 (in red) in REH2. Predicted α-helix (cylinders) and β-
916 strand (arrows) in REH2 are indicated.
917
918 **S5 Figure. Sedimentation analysis of endogenous editing proteins. (A)** 10-30% glycerol
919 gradients of freshly-made mitochondria-enriched extract from 29:13 procyclic trypanosomes.
920 Catalase and RECC complex were used as 11 S and 20 S markers, respectively (23).
921 Endogenous REH2, ^{H2}F1 and ^{H2}F2, GAP1 (GRBC2), GAP2 (GRBC1), and A2 (MP42) were
922 examined in western blots. All panels in this figure derived from the same extract fractions. The
923 data shown is representative of at least two panels for each protein in biological replicate
924 gradients.
925
926 **S6 Figure. Location of the zinc-finger substitutions examined in this study. (A)** Full ^{H2}F1
927 amino acid sequence including the location of eight C2H2 zinc-finger motifs (Znf1-to-8
928 highlighted in different colors)**. (B)** Zinc-finger motifs starting with the N terminal finger at the
929 top, and the amino acid positions spanning each finger in panel A. The R/K>A substitutions in
930 each finger that were examined in this study are marked by a dot.
931
932 **S7 Figure. RNase-resistant co-purification of tagged-^{H2}F1 and endogenous ^{H2}F1.** Western
933 blots of IgG pulldowns from extracts with or without an RNaseA/T1 mix. All panels in this figure
934 derive from the same blot. The upper blot with the tagged-^{H2}F1 bait was cut below the 75 kDa
935 marker. The middle and lower panels were divided between the 50 kDa and 37 kDa marker.
936 The 34.4 kDa RGG2, a typical subunit of the REMC module in the RESC complex. As expected,
937 the RNA-mediated association of RGG2 decreased with the RNase treatment.
938

939 **S8 Figure. Quantitation of steady-state RNA transcripts in the input mitochondrial**
940 **extracts used in the IgG pulldowns.** Independent biological replicates (two independent
941 cultures used in Fig. 5) with Cq average values and one standard deviation (+/-1SD, *n*=2) were
942 plotted. dCq of steady-state RNA transcripts in lysates relative to background 18s rRNA used as
943 reference [dCq = $2^{(\text{target Cq} - \text{ref Cq})}$]. Shorter bars indicate a smaller differential versus 18s rRNA in
944 the sample. For example, ND7 is relatively abundant compared to other transcripts in the
945 sample (i.e., it has a lower Cq). The WT construct is induced or not (+/-). All mutants are
946 induced. All end-point amplicons were examined in gels to confirm that they were single
947 products during linear amplification. Abbreviation of the RNA names is as in Fig. 5B.

948

949 **S1 Table. DNA oligonucleotides, gBlocks (IDT) and synthetic RNA.**

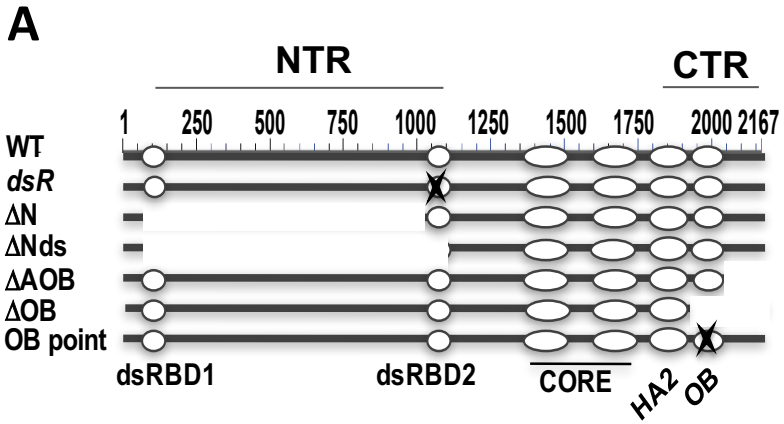

NAME	MUTATION	DOMAINS AFFECTED	MW
dsR	K1078A/A1086D	dsRBD2	242
ΔN	Δ34-1023	dsRBD1	132
ΔNds	Δ34-1093	dsRBD1/dsRBD2	124
ΔAOB	Δ1908-2167		228
ΔOB	Δ2045-2167	OB fold	213
1979	R1979A	OB fold	242
1998	H1998E	OB fold	242
1999	R1999E	OB fold	242
98/99	H1998E/R1999E	OB fold	242
2023	R2023A	OB fold	242

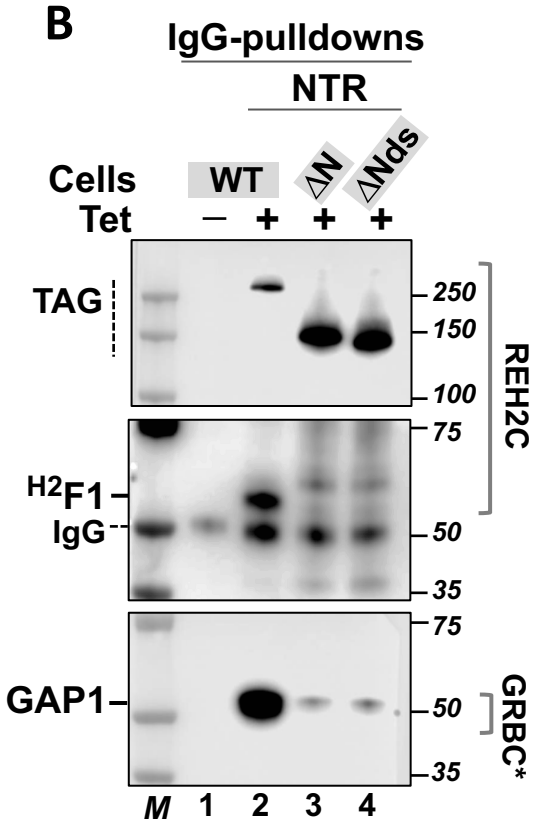

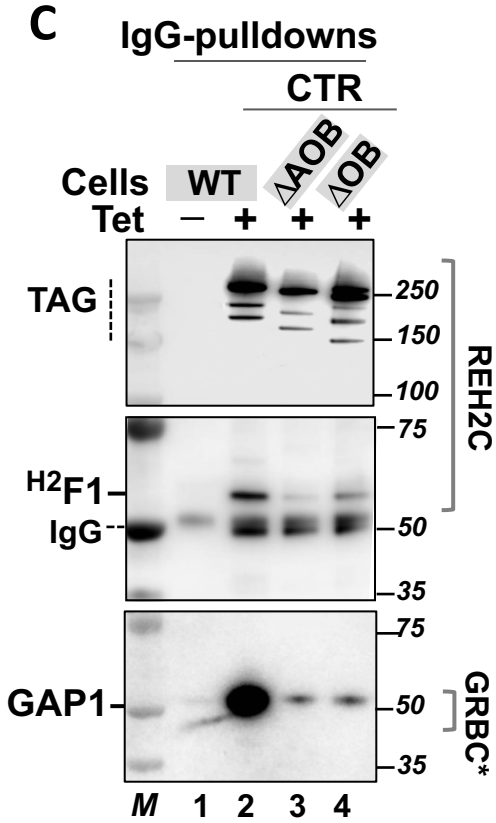

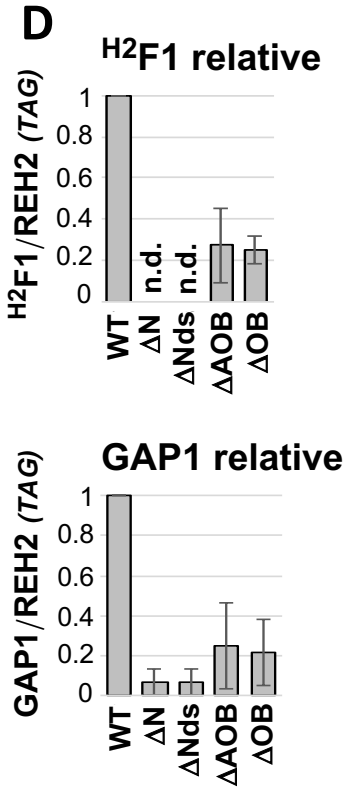

Figure 1

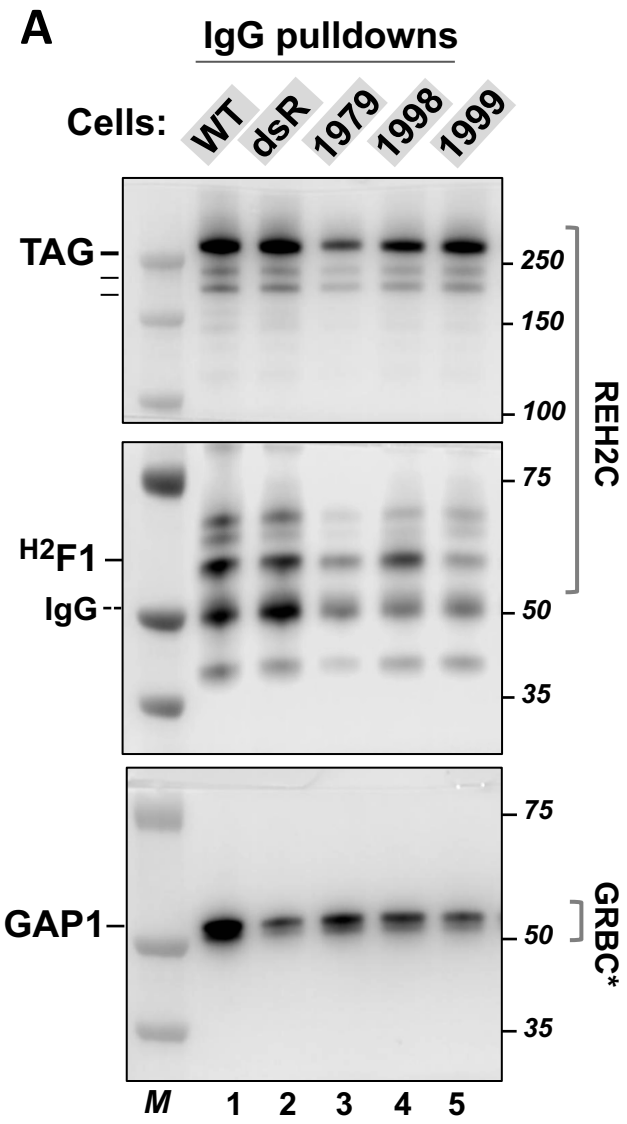
A
IgG pulldowns
Cells:
WT
dsR
1979
1998
1999
TAG
H2F1
IgG
GAP1
250
150
100
75
50
35
REH2C
GRBC*
M
1
2
3
4
5

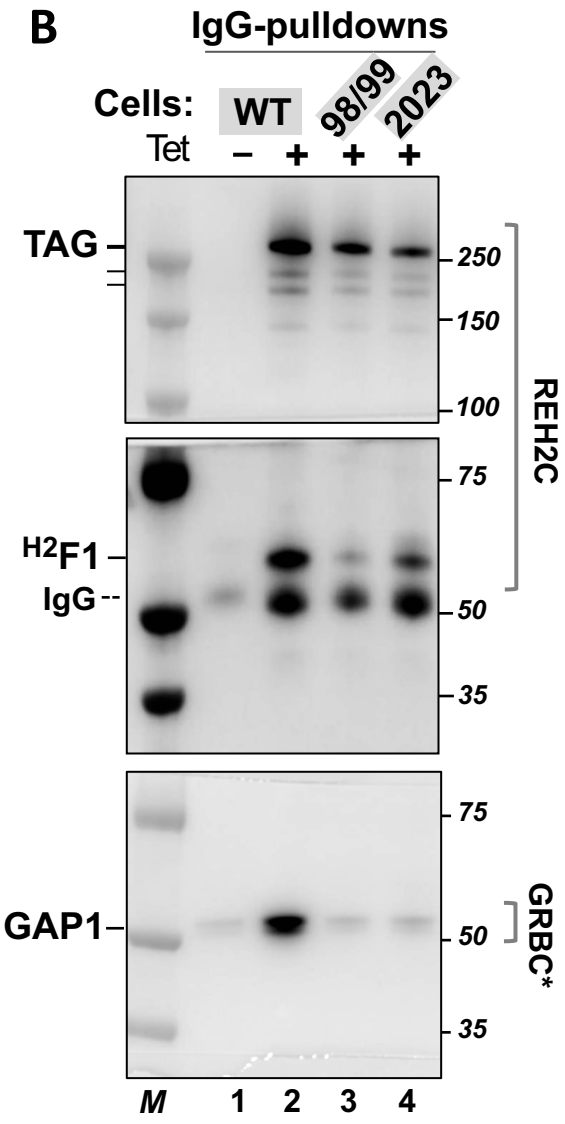
B
IgG-pulldowns
Cells:
WT
98/99
2023
Tet
–
+
+
+
TAG
H2F1
IgG
GAP1
250
150
100
75
50
35
REH2C
GRBC*
M
1
2
3
4

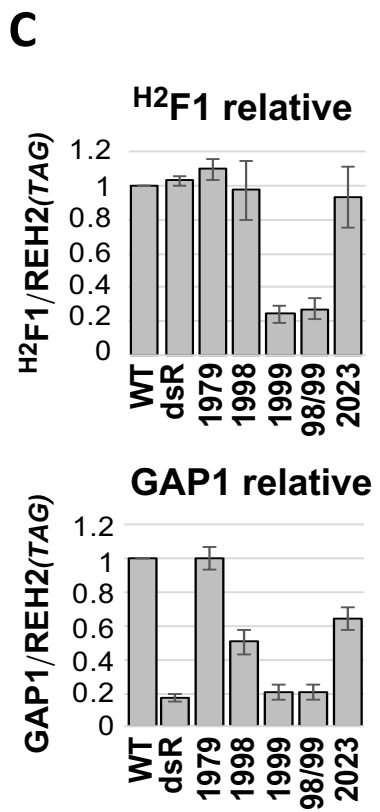
C
H2F1 relative
H2F1/REH2(TAG)
1.2
1
0.8
0.6
0.4
0.2
0
WT
dsR
1979
1998
1999
98/99
2023
GAP1 relative
GAP1/REH2(TAG)

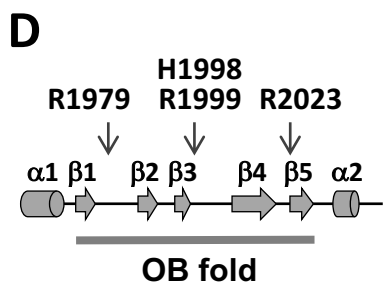
D
R1979
H1998
R1999
R2023
α1
β1
β2
β3
β4
β5
α2
OB fold

Figure 2

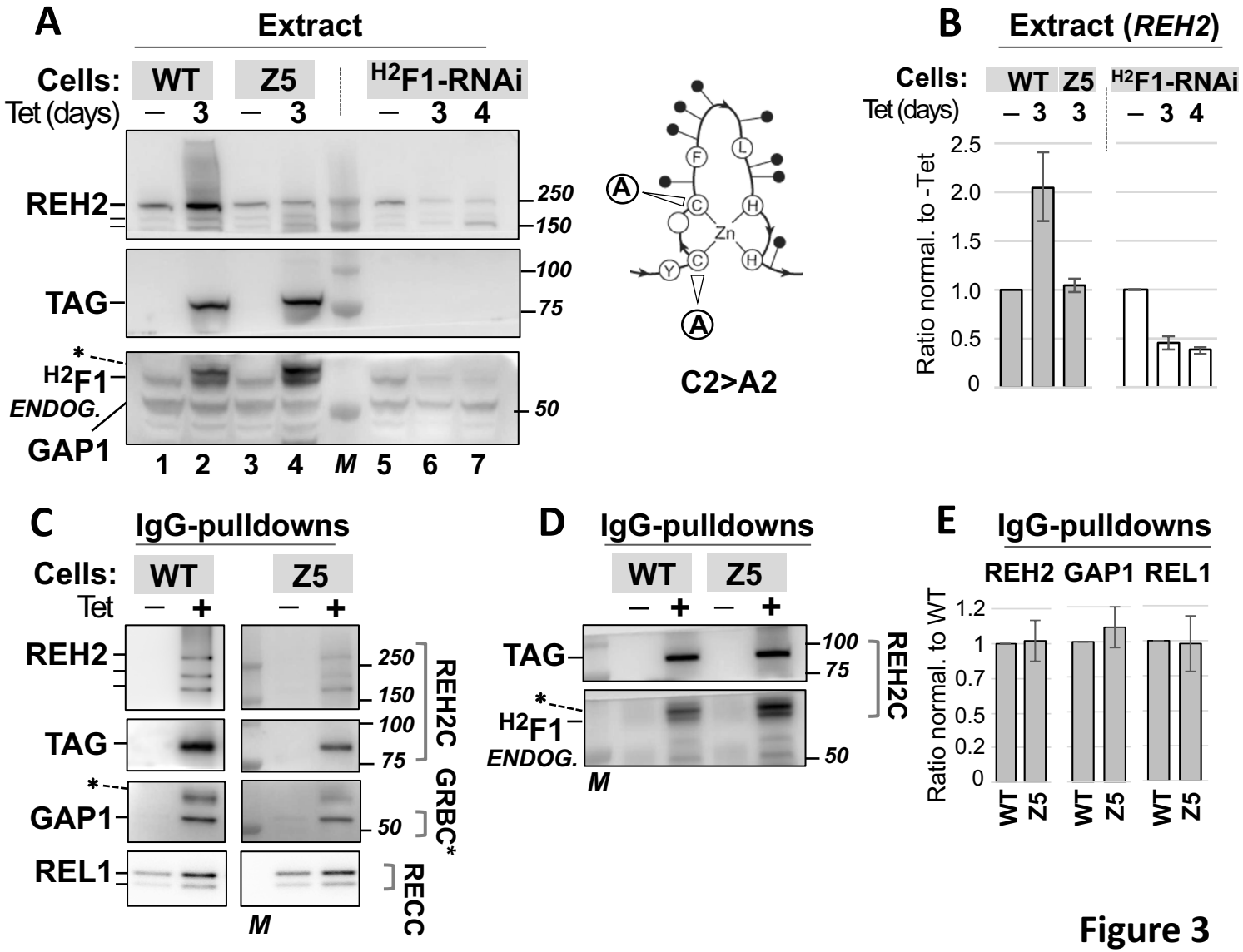
A
Extract
Cells: WT Z5 H2F1-RNAi
Tet (days) – 3 – 3 – 3 4
REH2
TAG
H2F1
ENDOG.
GAP1
250
150
100
75
50
1 2 3 4 M 5 6 7
C2>A2
B
Extract (REH2)
Cells: WT Z5 H2F1-RNAi
Tet (days) – 3 3 – 3 4
Ratio normal. to -Tet
2.5
2.0
1.5
1.0
0.5
0
C
IgG-pulldowns
Cells: WT Z5
Tet – + – +
REH2
TAG
GAP1
REL1
M
REH2C
GRBC*
RECC
D
IgG-pulldowns
WT Z5
– + – +
TAG
H2F1
ENDOG.
M
REH2C
E
IgG-pulldowns
REH2 GAP1 REL1
Ratio normal. to WT
1.2
1
0.7
0.5
0.2
0
WT Z5 WT Z5 WT Z5

Figure 3

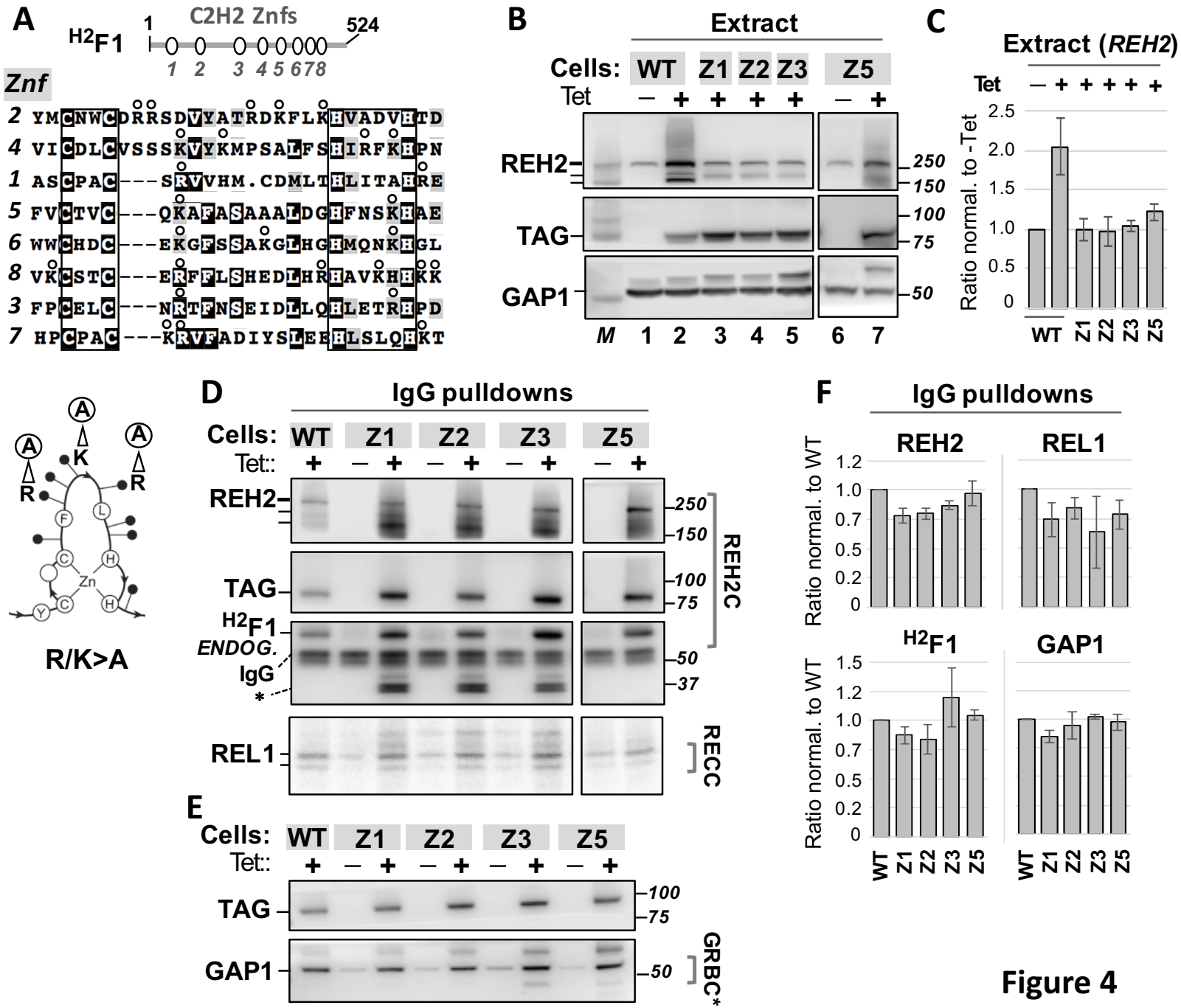
A
H2F1
C2H2 Znfs
1
524
1 2 3 4 5 6 7 8
Znf
2 YMCNWCDRRSDVYATRDKFLKHVADVHTD
4 VICDLCVSSSKVYKMPSALFSHIRFKHPN
1 ASCPAC---SRVVHM.CDMLTHLITAHRE
5 FVCTVC---QKAFASAAALDGHFNSKHAE
6 WWCHDC---EKGFSSAKGLHGHMQNKHGL
8 VKCSTC---ERFFLSHEDLHRHAVKHHKK
3 FPCELC---NRTFNSEIDLLQHLETRHPD
7 HPCPAC---KRVFADIYSLEEHLSLQHKT
B
Extract
Cells: WT Z1 Z2 Z3 Z5
Tet – + + + + – +
REH2
TAG
GAP1
250
150
100
75
50
M 1 2 3 4 5 6 7
C
Extract (REH2)
Tet – + + + + +
Ratio normal. to -Tet
2.5
2.0
1.5
1.0
0.5
0
WT Z1 Z2 Z3 Z5
A
K
R
R
F
L
C
H
Zn
Y
C
H
R/K>A
D
IgG pulldowns
Cells: WT Z1 Z2 Z3 Z5
Tet:: + – + – + – + – +
REH2
TAG
H2F1
ENDOG.
IgG
*
REL1
250
150
100
75
50
37
REH2C
RECC
E
Cells: WT Z1 Z2 Z3 Z5
Tet:: + – + – + – + – +
TAG
GAP1
100
75
50
GRBC*
F
IgG pulldowns
REH2
REL1
H2F1
GAP1
Ratio normal. to WT
1.2
1.0
0.7
0.5
0.2
0
1.5
WT Z1 Z2 Z3 Z5

Figure 4

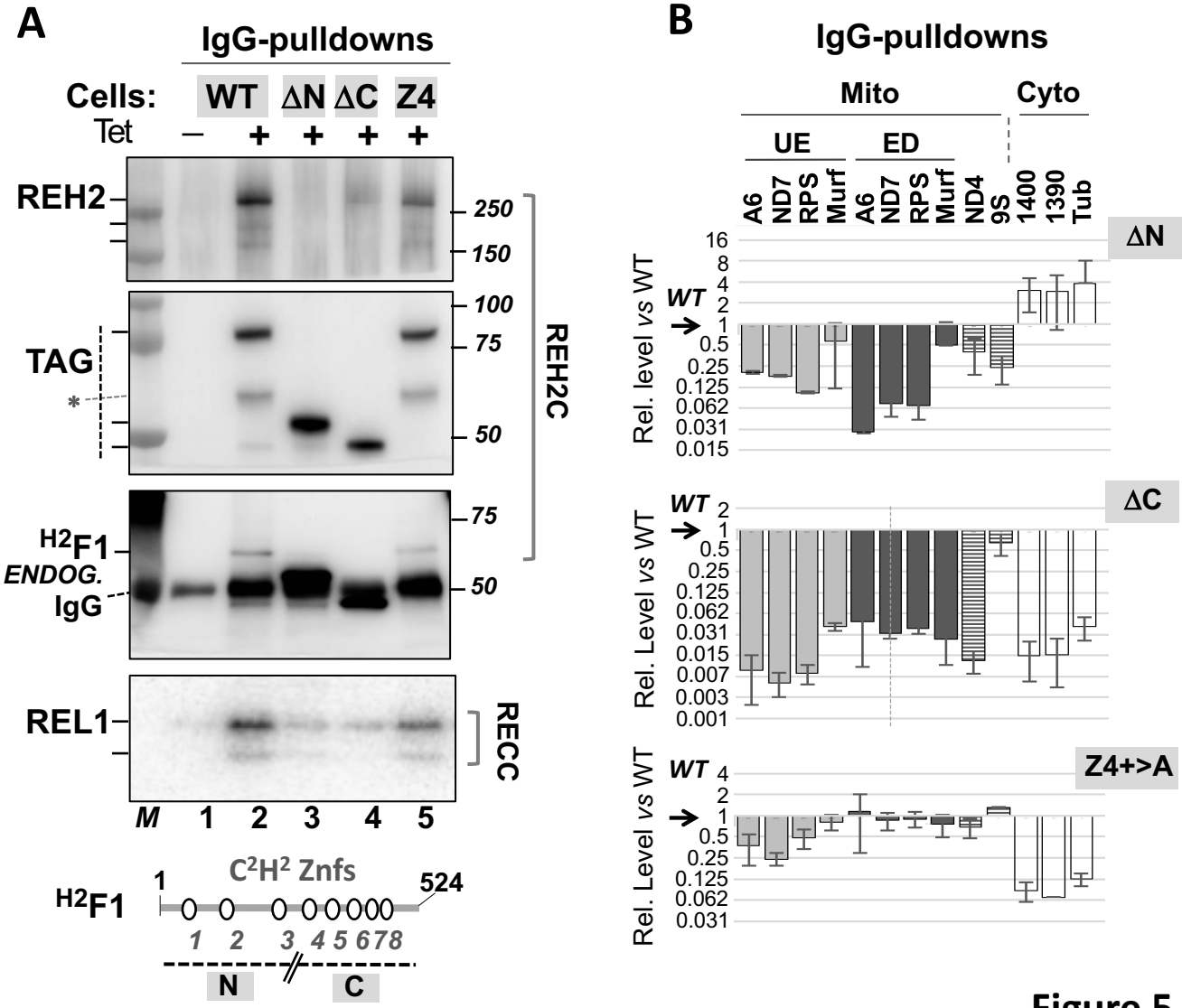
A
IgG-pulldowns
Cells:
WT
ΔN
ΔC
Z4
Tet
REH2
TAG
H2F1
ENDOG.
IgG
REL1
250
150
100
75
50
REH2C
RECC
M
1
2
3
4
5
C2H2 Znfs
524
N
C
B
Mito
Cyto
UE
ED
A6
ND7
RPS
Murf
ND4
9S
1400
1390
Tub
Rel. level vs WT
Rel. Level vs WT
WT
Z4+>A

Figure 5

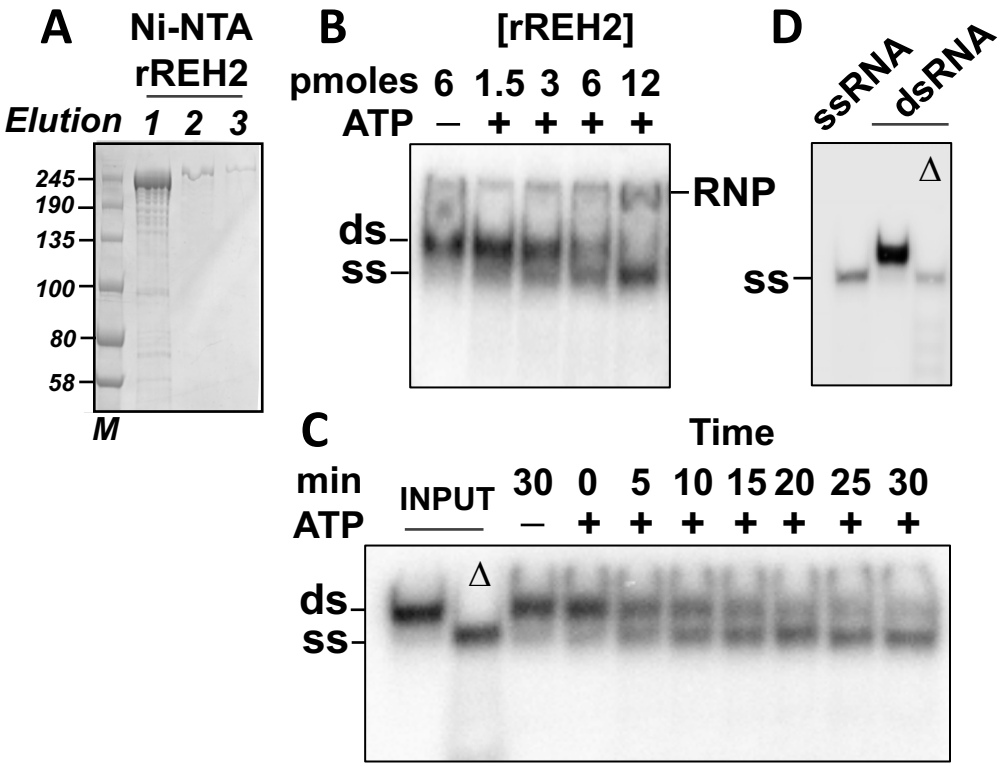
A
Ni-NTA
rREH2
Elution 1 2 3
245
190
135
100
80
58
M
B
[rREH2]
pmoles 6 1.5 3 6 12
ATP – + + + +
RNP
ds
ss
D
ssRNA
dsRNA
Δ
ss
C
Time
min INPUT 30 0 5 10 15 20 25 30
ATP – + + + + + + +
Δ
ds
ss

Figure 6